Modular steering mechanism design for cable guidance through reusable minimally invasive instruments

Remie Lether

MSc. Thesis

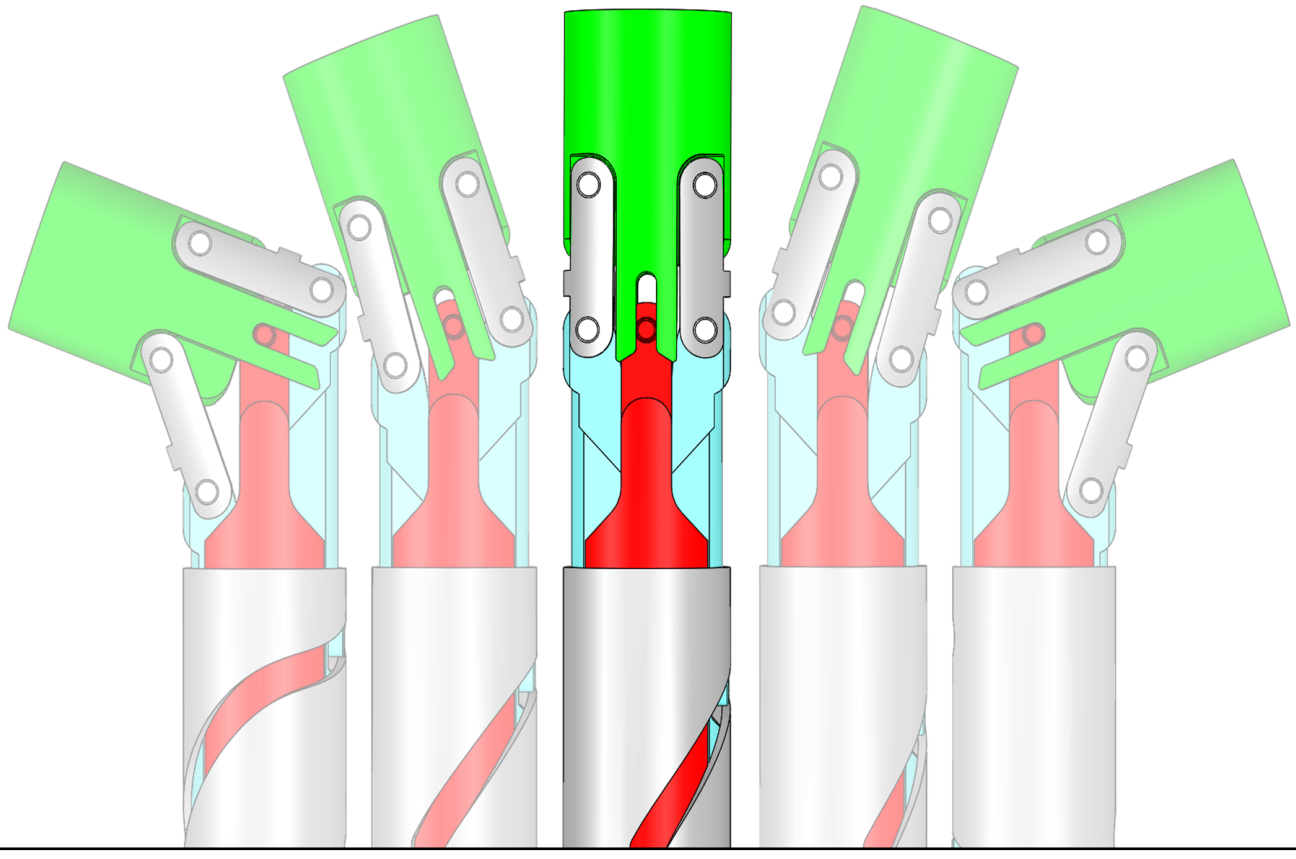

TU Delft Delft University of Technology

Modular steering mechanism design for cable guidance through reusable minimally invasive instruments

MSc. Thesis

To obtain the degrees of
Master of Science in Mechanical Engineering
Master of Science in Biomedical Engineering
at the Delft University of Technology.

Remie Lether

January 16, 2021

Supervised by

Department of BioMechanical Engineering:

Ir. T. A. Lenssen
Dr. Ir. T. Horeman

Department of Precision and Microsystems Engineering:

Ir. J. W. Spronck

Faculty of Mechanical, Maritime and Materials Engineering (3mE) · Delft University of Technology

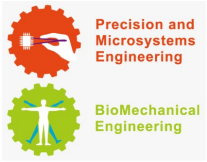

Table of Contents

Preface

During my Bachelor's thesis in Mechanical Engineering, I had the honor to work on a major challenge in minimally invasive surgery. In the project, fundamental mechanical principles were investigated to transfer high forces through small, flexible medical instruments, such as a catheter. The results of this research were published by Elsevier in the journal of Medical Engineering & Physics and familiarized me with the importance of technology used in the surgical scene. I got inspired by the application of mechanical engineering in minimally invasive surgery, which made me enroll for the masters Mechanical Engineering and Biomedical Engineering.

From personal experience, I know the importance of scientists pushing the boundaries of the medical field. Without biomedical research in the past, my future would have been different. After receiving medical treatment for years, it is a fair gesture for me to contribute to the medical field with knowledge I acquired at the Delft university of Technology.

Acknowledgements

Many people helped me in this graduation project, I owe them a word of thanks. The advises I received and the lessons learned from my supervisors were a valuable learning process to me.

First of all, I would like to say thanks to Tomas Lenssen for the seemly unlimited time he had as my daily supervisor. He shared his experience in designing laparoscopic instruments, which helped me create a feeling for Mechanical Engineering at the small scale of minimally invasive surgery.

I would like to thank Tim Horeman for the interesting research topic he proposed, it was a pleasure to study a mechanical device used in minimally invasive surgery. I felt encouraged by his eager and enthusiastic attitude, which pushed my graduation project to a next level.

I would like to express my gratitude for the directness and constructive feedback I received from Jo Spronck. In the weekly meetings we had, he highlighted the importance of vision and justification of decision making. These meetings were sharpening my mindset as a graduate student to become an open-minded Engineer.

I thank Quincy Chin-Chan-Sen for the information he shared regarding the manufacturability of my design. His experience as instrument maker was helpful to me.

After all, a word of thanks to fellow students, roommates and family who supported me with their peer reviews and inspiration.

Delft, University of Technology — Remie Lether
January 16, 2021

Abstract

Minimally Invasive Surgery (MIS) has made tremendous impact on hospitals worldwide. Introduced as a patient friendly alternative to open surgery by significantly reducing incisions size, benefits such as faster patient recovery time, and less pain for patients, are achieved. However, in MIS, rigid instrument shafts can impair surgeons' dexterity as access to pathology sites is complicated. Steering mechanisms have been developed to locate and orientate an instrument tip for tissue manipulation.

Many steerable Minimally Invasive (MI) instruments are intended for single use only, because the actuation cables in those instruments cannot be properly cleaned. Consequently, costly and well-functioning instruments are disposed after each surgical procedure, forming a burden to both hospital sustainability and financial expenses. A platform technology suitable for reuse is brought to the market by the Delft University of Technology in collaboration with Surge-On Medical B.V.

Problems with this platform arise in the integration of an internally routed cable, since a hinge in the steering mechanism leads to a critically small cable bending radius. In the present master's thesis, a bare minimum design approach is followed to make the platform technology compatible with internally routed cables. Based on set requirements, multiple concepts of steering mechanisms are generated and evaluated. The most promising concept is modelled, tested and validated with computer models and experiments. The final design comprises a four-bar linkage mechanism and an innovative joint is used to kinematically stabilize the mechanism. The mechanism achieves 140^o tip articulation and guides internally routed cables with a bending radius of 5mm. The steering mechanism fits through trocars of ∅5mm and can support loads of 40N, as applied by internally routed cables. The design can be integrated in reusable minimally invasive surgical instruments, since detachment of components allows for effective cleaning and inspection. The designed steering mechanism can be used as building block for reusable minimally invasive instruments, providing an important step to the next generation of steering technology in MIS.

Chapter 1

Introduction

1-1 Motivation

Minimally Invasive (MI) surgery has made tremendous impact on hospitals worldwide. Introduced as a patient friendly alternative to open surgery by significantly reducing incisions size, benefits such as faster patient recovery time, reduced infection risks, and less pain for patients, are achieved [1]. However, in minimally invasive surgery, long and rigid instrument shafts can impair surgeons' dexterity as access to pathology sites is complicated. Steering mechanisms have been developed to locate and orientate instrument tip with the organic shapes of anatomic structures [2].

Steerable versions of MI instruments are commonly intended for single use only, because the coiled structures of actuation cables used in those instruments cannot be properly cleaned [3]. These cables have crevices that can trap contaminants. Consequently, costly and well-functioning instruments are disposed after each surgical procedure, forming a burden to both hospital sustainability and financial expenses [4]. In numerous countries, cost on healthcare services are rising and form a source of debate. For example, in the Netherlands, governmental healthcare expenses have been increasing for decades and formed 13.1% of the gross domestic product in 2019 [5]. Financial considerations in hospitals are important to cut costs. Regarding MI surgery, reuse of instruments potentially results in financial benefit, since costs on instrument reprocess are expected to be lower than instrument purchase costs [4, 6, 7]. Therefore, the present graduation project is concerned with the design of a steering mechanism for reusable MI instruments.

1-2 Instrument anatomy

MI instruments use external actuators in combination with mechanical transmissions [8]. The basic components of conventional hand-held MI instruments, shown in Figure 1-1, are briefly presented. At the proximal side, instruments consists of a surgical handle that forms the control interface for surgeons. Long and rigid instrument shafts are used to access the abdominal cavity and to reach anatomic structures. Along these shafts, mechanical loads are transmitted between handle and tip. At the distal side, instruments are equipped with an end-effector used for

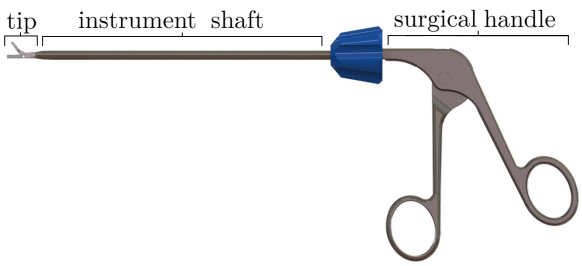

Figure 1-1: Anatomy minimally invasive instrument.

tissue manipulation. More sophisticated MI instruments are equipped with a steering mechanism that adds Degrees of Freedom (DoF) at the tip.

1-3 Overall Methods

This graduation project is at the cutting edge of Mechanical Engineering and Biomedical Engineering. These complementary study areas are represented in the design objective and the performed design methodology presented in this report. Fundamental principles of Mechanical Engineering are used to develop a steering mechanism composed of conventional mechanical components. Biomedical Engineering is predominantly found in the followed bare minimum design approach, where focus is set on the the integration of functionality in the long and rigid shafts of MI instruments [9]. As schematically depicted in Figure 1-2, the design approach is structured by distinctive design phases to allow for a systematic design process. It must be noted that the design process has an iterative character to guarantee integration and adoption of all design requirements [10].

1-4 Report Layout

Five distinctive design phases are presented throughout this report. In the first two chapters, background information on the design project is given and the design problem is defined. Corresponding to the design approach, these chapters are structured by a functional analysis and a list of design requirements. Chapter 3 is dedicated to steering mechanism morphology and conceptual design generation. Generated concepts are assessed in chapter 4 for substantiate concept selection. The most promising concept is elaborated in chapter 5, which yields the final concept design presented in chapter 6. Chapter 7 is concerned with final design validation and includes experimental results, numerical models and an overview of taken design measures. Finally, a discussion and conclusion are given on the result.

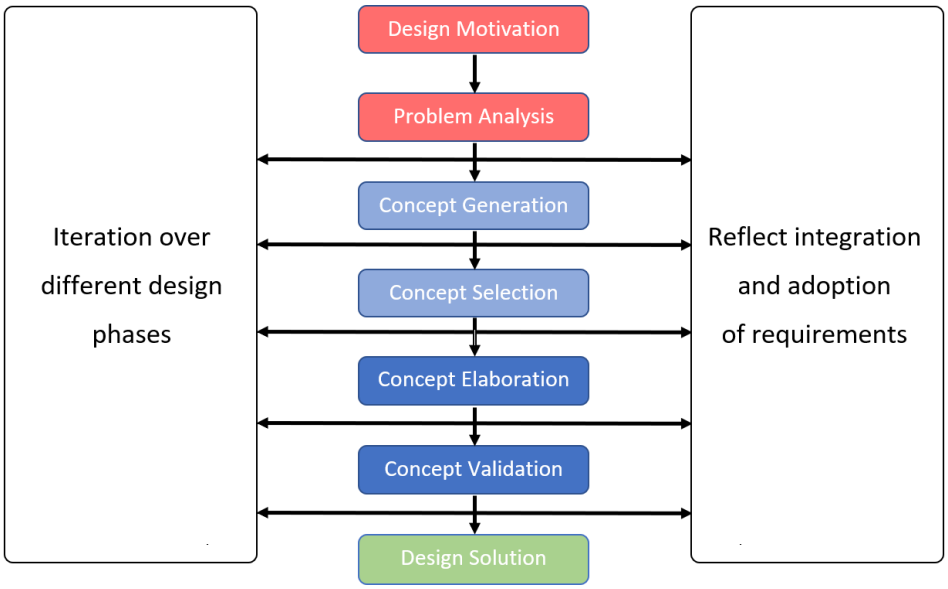

Figure 1-2: Schematic representation of the design approach.

Chapter 2

Problem Analysis

2-1 State-of-the-art Technology

Figure 2-1 shows the rigid shaft of a conventional MI instrument that permits 4 DoF, namely a translation through, and two rotations around the incision point (i.e., trocar), as well as a rotation around the instrument axis. Because of the rigid shafts, anatomic structures are approached via a straight line between pathology site and incision point. Surgeons' dexterity is impaired because conventional MI instruments lack 2 DoF to orientate the tip [11]. Steering mechanisms have been developed to add internal degrees of freedom such as tip rotation or tip articulation (schematically shown in Figure 2-2). In general, steering mechanisms are driven by cables with coiled structures that are hard to clean [3].

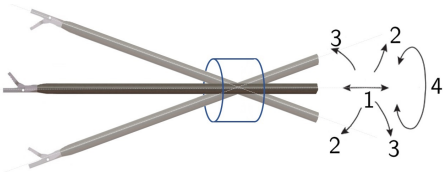

Figure 2-1: Degrees of freedom of conventional MI instruments. 1: linear translation through incision point. 2, 3: translation at the tip. 4: rotation around instrument shaft.

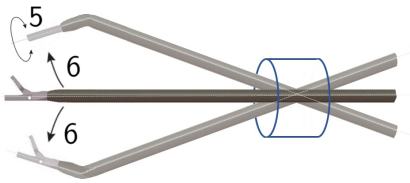

Figure 2-2: Examples of internal degrees of freedom of a steerable tip. 5: rotation of the tip. 6: tip articulation.

Continuum steering mechanisms (see Figure 2-3) typically consist of a flexible backbone structure actuated by antagonistic cables [12]. Alternatively, High-Degree-of-Freedom mechanisms consist of a rigid backbone structure composed of multiple rigid components that move relative to another [12, 13, 14]. A major drawback of backbone structures is the low end-point stiffness needed to support external forces exerted during tissue manipulation [11, 15, 16, 17].

Steering mechanisms with conventional mechanical components (shown in Figure 2-3) address some of the barriers of backbone structures because of the rigid joint design that improves on end-point stiffness. An example of such a mechanism is the Da Vinci Surgical System (Surgical Intuitive) [18] that achieves tip articulation with a single hinge. Actuation of the mechanism is done by antagonistic cable pairs, limiting the reusability of the system.

A cable-less mechanism with high end-point stiffness is the Shaft Actuated Tip Articulation (SATA) technology, developed at the Delft University of Technology in collaboration with startup company Surge-On Medical. The technology comprises of rigid linkages that allow for

a singe DoF tip articulation by shaft rotation as depicted in Figure 2-4 [19]. The mechanism is actuated by a cam-follower system, which induces a coupled linear translation of sliders. This simple mechanism provides high resistance to external tip loads as compared to backbone based mechanisms.

Figure 2-3: Examples of cable driven steering mechanisms. Left: backbone based articulation. Right: articulation by conventional hinges (Figure copied from [20]).

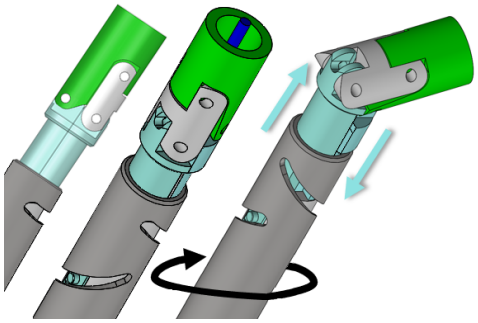

Figure 2-4: SATA principle: outer shaft rotation (black arrow) causes slider translation (turquoise arrows). Slider translation results in articulation of the (green) tip.

2-2 Bottleneck in SATA Technology

By design, SATA technology cannot comply with internally routed cables, since a hinge in the steering mechanism requires the cable to bend with a critically small radius, resulting in plastic deformation (shown in Figure 2-5-a). Backbone based steering mechanisms prevent plastic deformation of cables, since these mechanisms attain small curvatures that properly guide cables. A strategy to prevent plastic cable deformation in MI steering mechanisms is to subdivide single hinge rotation into smaller rotations of multiple hinges [13]. This strategy suits mechanisms composed of conventional mechanical components, thus subdividing hinge rotation can result in small internal cable curves and high end-effector stiffness. For example, in SATA technology, one additional linkage can provide space for cable bending without making compromises in terms of end-effector stiffness (Figure 2-5-b).

In the present master's thesis, SATA technology is redesigned to guide an internally routed cable without making compromises in terms of end-effector of the steering mechanism. In other words, this thesis project is aimed to *increase the bending radius of an internally routed cable with a redesign of SATA technology.*

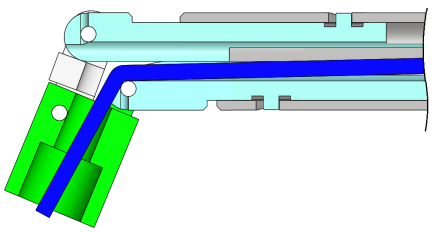

(a) Single hinge cable bending with critical bending radius.

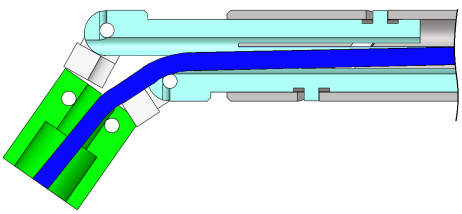

(b) Two hinge cable bending with improved bending radius.

Figure 2-5: Subdivision of hinge rotation leads to smaller curves in SATA's internally routed cables. Depicted cables (blue) are loaded by axial force.

Considering the internally routed cable as linear elastic material loaded by pure bending (i.e., ignoring axial forces and shear forces), the constitutive relations between bending radius (ρ), internal moment (M) and material stress (σ_y) at a distance y from the neutral axis can be expressed as [21]:

$$M = \frac{EI}{\rho} \tag{2-1}$$

$$\sigma_y = \frac{My}{I} \tag{2-2}$$

where the Young's modulus (E) multiplied by the cable's second moment of inertia (I) is known as the bending rigidity. The highest material stress (σ_{max}) is found at the location farthest away from the neutral axis. If this stress exceeds the material yield strength, plastic deformation occurs and the internally routed cable cannot fully recover from bending.

In reality, pure bending does not exist. In the application of cables routed through MI instruments, shear forces as well as axial forces are applied to the material, affecting both cable curvature and material stresses. Figure 2-6 depicts the situation where a SATA linkage forces an internally routed cable to bend around two distinctive hinges. The cable attains a gradual curve in the absence of axial loads, but is forced to bend with a small radius around two distinctive points if axial load is applied.

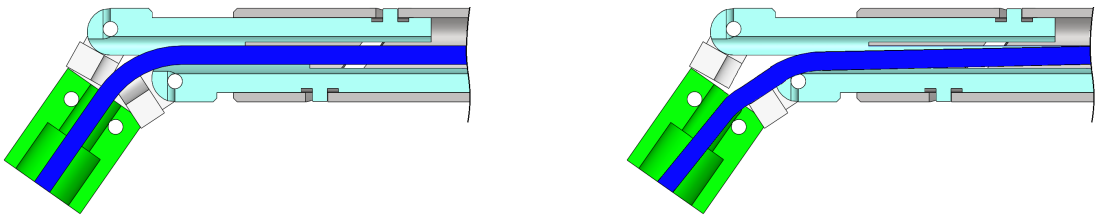

(a) No axial load applied. **(b)** Axial load applied.

Figure 2-6: SATA internally routed cable.

Although constitutive relations of Equation (2-1) - (2-2) do not accurately describe the case of an axially loaded cable, substitution of both equations reveals insights on the contribution of cable bending to material stresses. Bending stresses scale inversely proportional to ρ radius and directly proportional to both material property E and distance y. Here, the bending radius is affected by steering mechanism design [13], whereas the other two parameters depend on cable selection. In the remainder of this report, focus is set on increasing the bending radius by redesigning SATA technology.

2-3 Function analysis

Based on the SATA technology, a new articulation mechanism is to be found in the present thesis. Functionality of this mechanism is based on a MI procedure where instrument maneuverability is relevant, namely bipolar vessel sealing.

The bipolar sealer is an essential laparoscopic instrument used to achieve hemostasis (i.e., to control bleeding). At the instrument tip, bipolar vessel sealers comprise a grasper to compress tissue. Two grasper jaws are electrically insulated from each other and connected to a power source (the advanced electrosurgical unit). Hemostasis is achieved by compressing targeted anatomic structures and applying an altering current to raise tissue temperature [22]. The bipolar vessel sealer is used in a number of minimally invasive procedures such as gynecology [23, 24, 25] and visceral surgery [25, 26, 27]. According to the Medical Devices Regulation 2017/745, Annex VIII, Chapter I [28], the bipolar sealer is an invasive instrument to be inserted inside patients through a surgical incision. The surgical instrument is intended for transient use, meaning that it invades the patient up to 60 minutes.

To achieve high quality surgical outcomes, proper alignment of instrument tip and targeted anatomic structures is needed [29]. In general, bipolar vessel sealing is done by: 1) aligning instrument with tissue, 2) compressing tissue with the surgical grasper, 3) coagulating tissue by radio-frequency current, and 4) retracting the instrument [30, 22].

From a technical point of view, bipolar vessel sealing is comparable to object gripping in robotics. Here, the orientation and position of the objects (i.e., anatomic structures) determines the trajectory needed to locate the gripper (i.e, grasper) [31, 32]. A total of 6 DoF describe the orientation and position of an object. As discussed in Section 2-1, rigid instrument shafts impair surgeons' dexterity as access to pathology sites is complicated. Instruments with a steering mechanism improve on dexterity since they have an internal DoF suitable for tip orientation. Therefore, the steering mechanism must serve the following main-function:

The steering mechanism should achieve tip articulation.

The main-function of the articulation mechanism must incorporate the following sub-functions:

- *The mechanism must be usable in laparoscopic procedures.*
  Rationale: it is intended to invade patients via small portals.
- *The mechanism must be reprocessable.*
  Rationale: This graduation project is targeted to design a reusable steering mechanism. For reuse, instrument reprocess is needed in the form of instrument cleaning, inspection, maintenance, and sterilization.
- *Achieve tip articulation from linear motion.*
  Rationale: SATA technology is based on a cam-follower system that provides linear motion as input for tip articulation.
- *Transmit translations over a variable angle.*
  Rationale: to actuate the surgical grasper independent of tip articulation.
- *Comply with an internally routed cable.*
  Rationale: to avoid critically small cable bending radii (Section 2-2).

2-4 Design Requirements

Design requirements are set to secure quality of performance and to understand both cost and values of design parameters. The Tom Gilb method [33] is used to obtain and quantify objective design requirements that allow for validation in a later design phase. As such, a description, physical unit, validation method, targets, and rationale are given per requirement. Requirements are defined in three categories: **A** Dimensional requirements, **B** Mechanical requirements, and **C** Requirements for reprocess.

A: Dimensional requirements

- **Requirement A1**
  Description: The outer diameter of the mechanism must fit a standard trocar for ∅5 mm instruments.
  Scale: [mm]
  Validation: Check the outer dimension of the detailed design.
  Targets:
  - Must do: ∅5.3 mm
  - Plan: ∅5.0 mm
  - Wish: $<$ ∅5.0 mm
  Rationale: The most prevalent trocar is suitable for 5mm instruments [20]. Smaller instrument diameters can lead to smaller incisions.

B: Mechanical requirements

- **Requirement B1**
  Description: Provide tip articulation.
  Scale: [^{o}]
  Validation: Analyse the range of motion of a prototype.
  Targets:
  - Must do: $\pm 55^o$
  - Plan: $\pm 60^o$
  - Wish: above $\pm 60^o$
  Rationale: The original SATA steering mechanism is designed for 55^o tip articulation [19]. However, modern vessel sealers such as the Da Vinci® Energy Vessel Sealer Extend from Intuitive Surgical, Inc. have articulation angles up to 60^o [18].

- **Requirement B2**
  Description: Transmit adequate force for blood vessel compression.
  Scale: [N]
  Validation: Use a prototype or computer model and representative apply load.
  Targets:
  - Must do: 20N
  - Plan: 40N
  - Wish: $>$ 40N
  Rationale: Scientific studies suggest that 20N grasping force results in optimal seal quality in vessels of 7 mm [34]. Cable forces are higher because of transmission ratios in the instrument. A robust steering mechanism has a margin force before failure.

- **Requirement B3**
  Description: The cable bending radius must be larger that five times the cable diameter.
  Scale: [mm]
  Targets:
  - Must do: $5 \cdot d$
  - Wish: $\geq 5 \cdot d$
  Validation: Validate with prototype.
  Rationale: This requirement is in accordance with the rule of thumb used in the study of Sakes *et al.*[35]

- **Requirement B4**
  Description: No mechanism singularity is allowed.
  Scale: [-]
  Validation: Use a prototype to validate the absence of singular positions.
  Rationale: At singular positions, the surgeon is unable to actuate the steering mechanism.

C: Requirements for reprocessing instruments

- **Requirement C1**
  Description: Modular design.
  Scale: [-]
  Validation: Validate with a prototype that the mechanism can be (dis-)assembled.
  Rationale: Detachment of components provides access to hidden lumen for inspection, rinsing and brushing [3, 19].

- **Requirement C2**
  Description: Prevent misassembly of instrument.
  Scale: [-]
  Validation: Ensure that there is only one way to connect the interfaces of the steering mechanism.
  Rationale: Single fit of components results in inherent safety by design.

- **Requirement C3**
  Description: Components interfaces must consist of sloping corners.
  Scale: [-]
  Validation: Check edges at interfaces.
  Rationale: For assembly, edges allow for easy components positioning [19].

- **Requirement C4**
  Description: No coiled cable structures are allowed in the design
  Scale: [-]
  Validation: Validate the absence of coiled cables in the detailed design.
  Rationale: Contaminants can accumulate in the cervices of cables, reducing the safe lifespan of reusable instruments by the risk of patient cross-contamination [3].

- **Requirement C5**
  Description: The mechanism should be composed of autoclavable components.
  Scale: [-]
  Validation: Validate for each component if it is used in autoclavable surgical instruments.
  Rationale: A reusable device is ought to resist the hard environment of the autoclave [3, 9].

Summary

In general, steerable laparoscopic instruments are intended for single use only, since they comprise of actuation cables that cannot be cleaned properly. Steering mechanism are either based on backbone structures or conventional hinges, where the latter is known for a high end-point stiffness. One cable-less MI steering mechanism with high end-point stiffness is the SATA technology, suitable for reuse. In the present master's thesis, SATA technology is redesigned to make the articulation mechanism suitable for internal cable routing. A functional analysis is performed to define mechanism functionality. To secure quality of performance and to understand both cost and values of design parameters, quantitative and qualitative design criteria are defined.

Chapter 3

Conceptual Design

In this chapter, the generation of conceptual solutions is presented. This process is initiated by exploring the fundamental principles behind the SATA articulation mechanism. Based on this, a number of features is selected to preserve for redesign. Further, fundamental design principles used in steerable laparoscopic instruments are analyzed to construct a morphological chart from which a number of design solutions is generated.

3-1 Degrees of freedom

SATA technology is based on a linkage mechanism, consisting of three hinges, one linkage and two sliders that define the kinematic relation between instrument shaft and tip. Synthesis of a linkage mechanism is done to achieve desired system kinematics and allows for a vast amount of mechanism topologies that can be categorized as function generators, path generators, and motion generators, respectively [36]. Function generators relate certain mechanism inputs (e.g., actuation force) to required outputs (e.g., end-point force). In case of path generation, a set point at the mechanism must follow a specified path. When requirements are set on both path and pose of a mechanism member, a motion generator is needed. SATA articulation mechanism is a motion generator, since it controls the pose of the end-effector.

According to the Chebychev–Grübler–Kutzbach criterion [37], the original SATA articulation mechanism has two DoF. By definition, this system is kinematically determinate, since two actuation forces (exerted by the outer shaft) control two degrees of freedom. Since the minimum required number of actuation force is used to control the degrees of freedom, the system is said to be exactly actuated [38].

In exactly actuated systems, intended motion is controlled while other degrees of freedom are constrained. As such, design complexity is minimized and end-point stiffness is high. Compared to overactuated systems, this system is more robust in terms of alignment and path variation, but has a lower load capacity [38, 39]. Considering that the steering mechanism is to be (dis-)assembled, some robustness in alignment and path variation is required. Therefore, the principle of exact actuation is preserved in SATA technology.

It appears that one additional linkage in the SATA technology provides space (potentially usable) for cable bending, but introduces an internal degree of freedom in the form of parallel linkage motion (shown in Figure 3-1). In case of an internal DoF, position changes can lead to adverse events related to end-point position accuracy and operational time [38]. In the remainder of this report, this motion will be referred to as (kinematically) unstable, since it is an unintended motion that must be controlled. This leads to the following design strategy:

An additional link forms the starting point of the SATA redesign and gives rise to the design of an extra joint to constrain one degree of freedom.

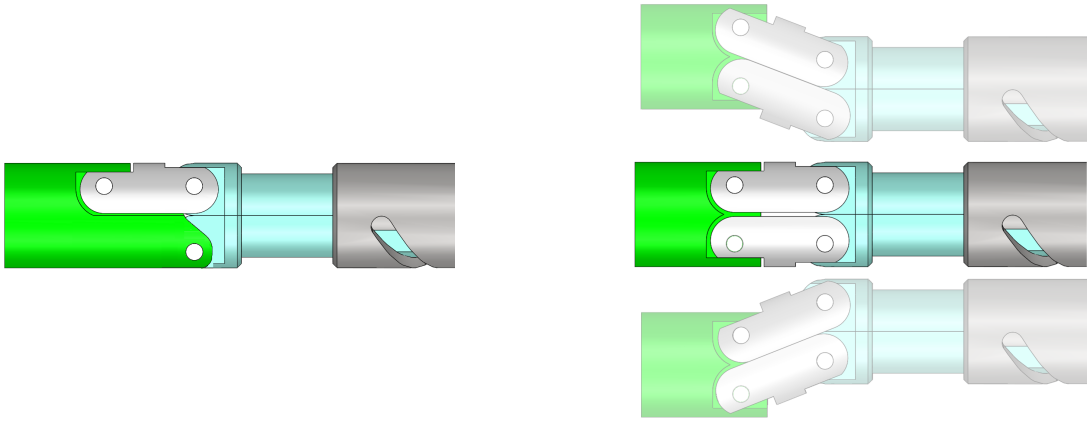

(a) No internal degree of freedom in original SATA.

(b) Internal degree of freedom by extra linkage.

Figure 3-1: Internal degree of freedom in SATA introduced by extra linkage.

Difficulties arise in the location of the needed kinematic constrain, since it requires an extra joint between tip and instrument shaft. This joint is to be detached for cleaning and inspection, which demands for a modular joint design. SATA technology is based on a proven assembly procedure [9], where shafts slide over another. The extra kinematic constraint must be designed such that axial separation of the joint interfaces is possible to allow for the same instrument detachment method as SATA technology. Notice that unintended axial joint separation during operation can be prevented by the kinematic constraints provided by both SATA linkages.

3-2 Design Principles

Prior to redesigning SATA technology, an overview of design principles suited for MI instruments is generated. The overview is organized based on the sub-systems of a steering mechanism.

3-2-1 Structural Architecture

System kinematics are set by the structural architecture of the steering mechanism. Distinctive principles use different types of joints that potentially stabilize (i.e., constrain) the internal DoF created by the addition linkage in the SATA articulation mechanism. In academic literature, three distinctive structural architectures are found: linkages, flexible backbones, and rigid backbones [8, 14]. These principles, shown in Figure 3-2, are introduced and discussed below.

- **Linkages:** The number of degrees of freedom of these mechanisms is given by the Chebychev–Grübler–Kutzbach criterion [37] and depends on the number of bars and hinges. In the absence of internal degrees of freedom, linkage based steering mechanisms benefit from high end-point stiffness due to the rigid joint design. These joints provide

torsional stiffness and prevent separation of joint interfaces (i,e, joint split) in both axial and transverse direction [14, 13]. Miniaturization of linkage systems is challenging as mechanism synthesis is confined by the small scale of a laparoscopic device, due to the restricted instrument outer diameter of ∅5mm. A simple linkage mechanism is shown in Figure 3-2-A.

- **Flexible backbones:** Joints in the form of flexible backbone structures can adopt infinitely many poses and therewith improve surgeons' dexterity significantly. By definition, control of this mechanism is underactuated, since flexible structures can be considered as infinite DoF systems. Herewith, flexible backbones can attain complex poses, like the s-curve depicted in Figure 3-2-B. With this technology design challenges are related to backbone buckling and low end-point stiffness [17, 40].
- **Rigid backbones:** With this technology, tip articulation is caused by relative motion between multiple rigid backbone segments (see Figure 3-2-C). A paradoxical problem arises for each extra added backbone segment: on the one hand, additional segments reduce curvature of internal cables, on the other hand, additional segments destabilize the steering mechanism as they introduce internal degrees of freedom and reduce end-point stiffness. Control of internal degrees of freedom is therefore an important design parameter for backbone structures. Jelínek *et al.* [14] categorized backbone interface types based on the fundamental mechanical design and working principle of the articulation. At the interface between segments, either bending, rolling, sliding, or a combination of rolling and sliding motions occur.

Selected architecture:

Linkage mechanisms are composed of hinges that provide two degrees of constraint and are likely to result in high end-point stiffness to the articulation mechanism. Hinges provide one more degree of constraint than intended. The kinematic redundancy of flexible backbone joints cannot be exactly actuated, thus is expected to provide low end-point stiffness. Design challenges with rigid backbone structures arise in the control of internal degrees of freedom to obtain end-point stiffness. Notice that the proposed SATA redesign requires a single joint to constrain one internal degree of freedom, meaning that end-effector stiffness is already achieved in five directions. To ensure sufficient freedom for concept generation, joint designs based on flexible and rigid backbone structures are used to develop conceptual solutions.

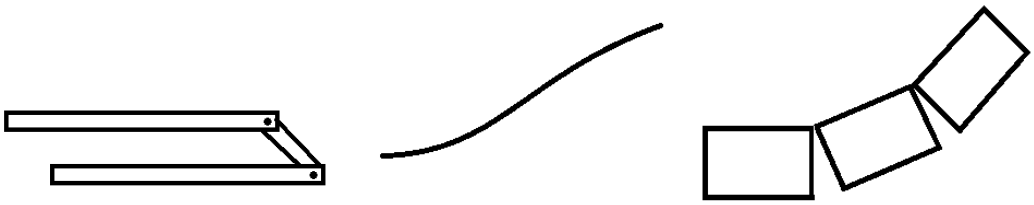

(a) Linkages **(b)** Flexible backbone **(c)** Rigid backbones

Figure 3-2: Schematic representation of mechanism structural architectures.

3-3 Concept Generation

This section is devoted to the generation of conceptual design solutions to increase the critically small cable bending radius. To structure the design approach, an overview of design principles is generated in the form of a morphological chart as included in Table 3-1. Each of the included design solutions is deduced from the fundamental principles selected in the previous chapter. The combination of different solutions brings a variety of concept designs.

Table 3-1: Morphological Chart

	Solutions							
	A	B	C	D	E	F	G	H
backbone joint	double-nested joint 	nested joint fully covered 	centered nested joint 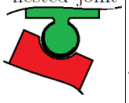	none 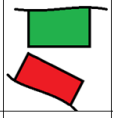	notch joint 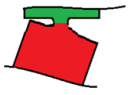	leaf flexure 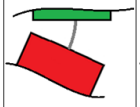	crossed flexures 	rolling contact 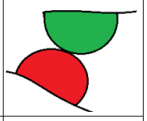
bar mechanism	single crank 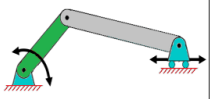	double-crank 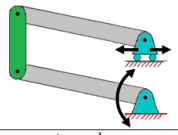						
degree of actuation	single degree 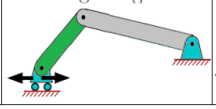	two degree 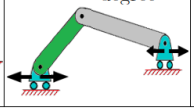						

3-3-1 Concepts

Figure 3-3 depicts the generated concepts. All concepts are exactly actuated, meaning that the number of actuation inputs equals the number of mechanism DoF. All concepts consist of a (green) tip, a (red) inner shaft, (turquoise) sliders, and (silver) linkages. It is assumed that the inner shaft is stationary, therefore, the inner shaft is considered as fixed frame. A distinction can be made between crank based and double-crank based mechanisms, since concepts (c) - (f) include only one linkage (i.e., crank), whereas the remainder of concepts consist of two linkages. Those concepts with two linkages are considered as hybrid systems, since the concepts are composed of a linkage mechanism stabilized by joint principles obtained from backbone based articulation mechanisms. Hinges at both mechanism sides provide torsional stiffness to the steering mechanism and prevent axial and transverse slip of components. It is chosen to locate the extra kinematic constraint at the medial instrument side, such that it is located between the linkages. Because of this location, the constraint will be referred to as inner joint in the remainder of this report.

Interfaces of the inner joint experience a relative motion during tip articulation. As such, concepts can be grouped by inner joint principle:

- *Sliding motion:* Sliding motion along the surfaces of the inner joint in concepts (a) and (b) results in joint motion. The joint interface consists of mutually fitting curved surfaces through which transverse joint split is prevented [14].

- *Material compliance:* The inner joints of concepts (c) - (f) are based on elastic material deformation, which allows for a monolithic inner joint design. In essence, these joint concepts act as a spring and need continuous force input to remain in position. If not actuated, the mechanism returns to the configuration with the lowest elastic energy storage. The joint characteristics are determined by its dimensions and material properties [41]. Regarding degrees of freedom, a single linkage is sufficient for a kinematically determinate system.
- *Rolling motion:* Concepts (g) - (i) achieve relative motion by rolling. Concept (g) comprises gear teeth to prevent slip, making the system independent from friction. Sufficient normal force at the joint interface of concept (h) is necessary to prevent slip, whereas concept (i) uses belts to prevent slip [42]. Concept (i) is monolithic and requires only a single linkage to make the system kinematically determinate.

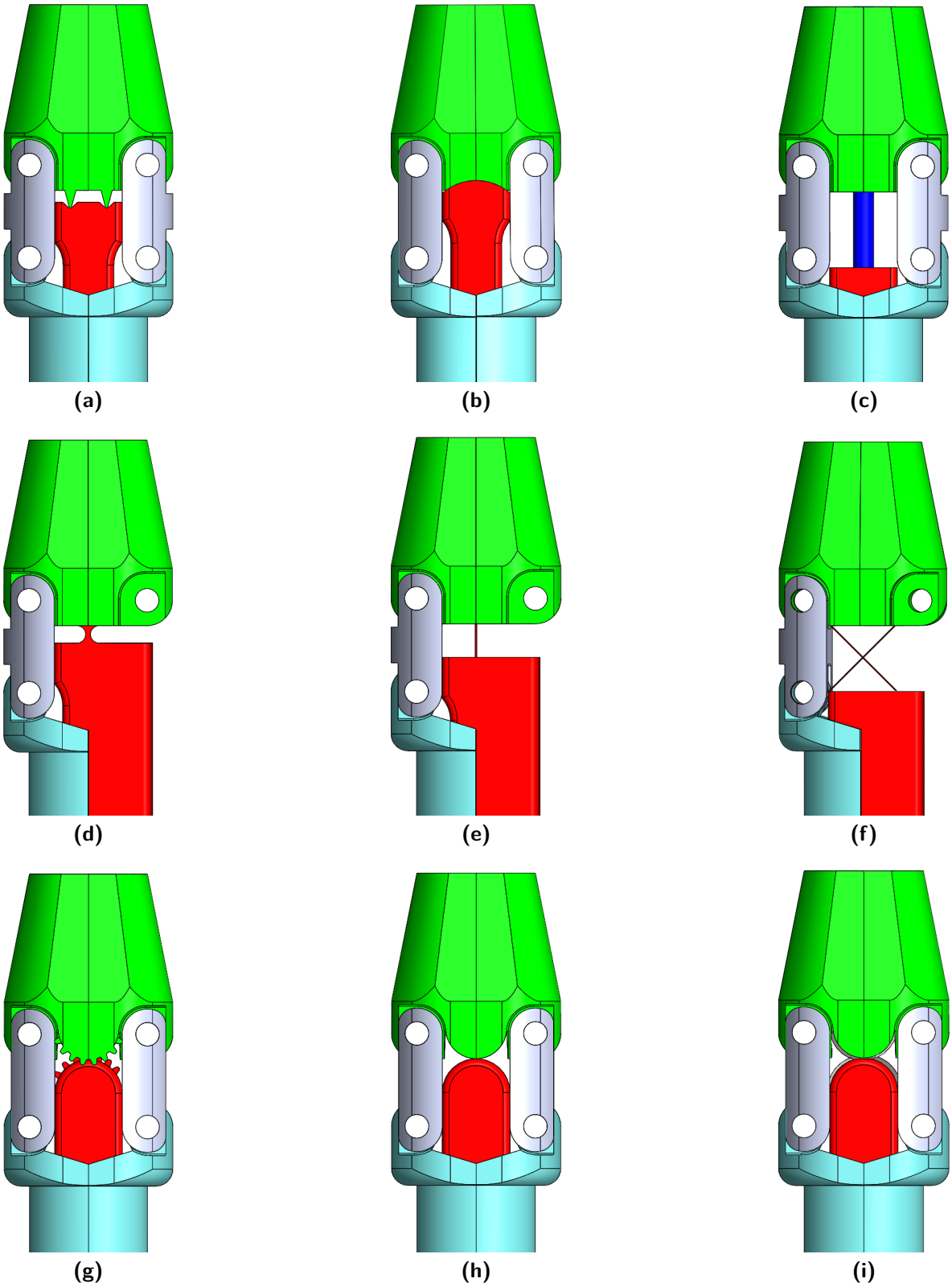

Figure 3-3: Conceptual solutions: (a) Double nested joint, (b) Single nested joint, (c) Cable support, (d) Notch joint, (e) Leaf flexures, (f) Crossed leaf flexures, (g) Gear, (h) Rolling contact, (i) Compliant rolling contact.

Chapter 4

Concept Selection

Strength and weaknesses of the generated concepts are evaluated in this chapter to select the most promising concept for elaboration. Concepts are systematically compared and discussed, which is graphically represented by the Harris profile provided in Table 4-1.

4-1 Evaluation criteria

Mechanical performance and device cleanability are evaluated by set criteria. Both expected cable bending radius and inner lumen play are used to assess cable curvature. The first is associated with intended displacement of the steering mechanism, the latter with play between cable and inner lumen. Force resistance is the criterion stating how well the inner joint constrains the internal DoF of the articulation mechanism. Robustness of the inner joint is used to asses joint performance in case of dimensional variations. The Range of Motion (RoM) of concepts is assessed as measure for surgeons' dexterity improvement. Regarding device cleanability, the number of hidden surfaces is evaluated.

4-2 Results and interpretation

To interpret the importance of distinctive functionalities, essential criteria are given a weight factor 2. The remaining criteria are given a factor 1. Those concepts assessed with -2 for any criterion are considered unfeasible to meet the design requirements. This systematic approach is represented by the Harris profile below (Table 4-1, enlarged in Appendix A). The profile reveals concepts (e) and (f) as most promising with an overal score of 11 and 12, respectively.

Table 4-1: Harris profile

		Concepts								
Criteria	**Weight**	**(a) Double nested joint**	**(b) Single nested joint**	**(c) Cable support**	**(d) Notch**	**(e) Leaf flexure**	**(f) Crossed leaf flexure**	**(g) Gear**	**(h) Rolling contact**	**(i) Compliant rolling contact**
Bending radius	2	2	-1 2	2	-1 2	2	2	2	2	2
Play inner lumen	1	1	2	-2 2	2	2	2	-1	1	-1
Range of motion	1	-1	2	2	-2	1	1	2	1	2
Force resistance	1	1	2	-2	1	-2	-1	2	-2	2
Robustness inner joint	1	-1	1	1	2	2	2	2	-2	2
Hidden surfaces	2	1	1	1	1	2	2	-1	1	-2
	Score	**6**	**8**	**3**	**4**	**11**	**12**	**7**	**8**	**7**

4-3 Comparison and discussion

Available information on conceptual designs is collected. Different criteria are used to generate comparable insights on concepts needed for substantiated concept selection.

4-3-1 Bending radius

The internally routed cable is bend around one specific point that is referred to as Bending Center (BC). In the present analysis, the BC is based on relative motion between instrument shaft and tip. To reduce cable curvature, the BC is to be placed as far from the instrument axis as possible. Figure 4-1 depicts the cable BC (yellow dot) in relation with tip articulation, lateral tip displacement and the distance between frame and tip. In this analysis it is assumed that the cable is free to move (i.e., there is clearance between cable and instrument). A lateral displaced tip with a large distance between frame and tip results in a BC most applicable for small curvature cable bending.

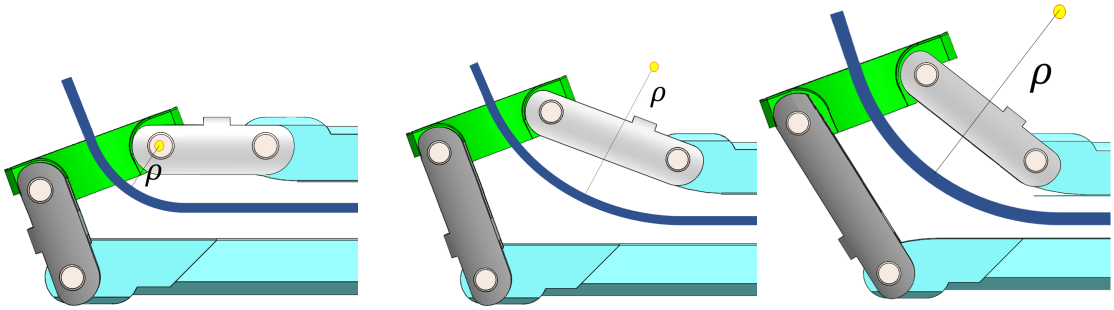

(a) No lateral tip displacement, small bending radius.

(b) Lateral tip displacement potentially increases cable bending radius.

(c) Combination of lateral tip displacement and long linkages potentially increases cable bending radius.

Figure 4-1: Relation between displacement of the tip and the cable bending radius (ρ).

- **Concept (a):** With two inner joints located at the lateral side of the instrument, the center of rotation of the tip does not coincide the instrument axis. This causes lateral displacement of the tip and increases space for cable bending.
- **Concept (b):** The sliding motion between frame and tip follows a circular path. Consequently, lateral displacement of the tip is negligible, leaving limited space for cable bending. Axial distance between hinges and nested joint potentially increases lateral tip displacement needed for cable bending.
- **Concept (c):** With the internally routed cable used to constrain the internal DoF, the tip follows the bending radius of the cable. As such, this conceptual solution provides sufficient space for cable bending.
- **Concept (d):** A notch joint can be considered as (compliant alternative of a) hinge. Here, the BC is at the instrument axis, leaving limited space for cable bending. However,

multiple notch joints can be stacked through which the range of motion is extended and the BC is relocated in lateral direction.

- **Concept (e):** Material bending of leaf flexures is used as steering mechanism. Hence, this mechanism offers sufficient space to cable bending.

- **Concept (f):** Cross-flexures are the compliant equivalent of a rolling joint [43]. The Center of Rotation (CoR) of the joint is located at the crossing point of the flexures, providing a lateral displacement of the tip needed for cable bending. Herewith, amplification of lateral movement is caused by the distance between crossing point and tip.

- **Concept (g) - (i):** These concepts comprise a rolling motion with a CoR present at the interface between both joint members. The roller's radius equals the amplification of lateral tip displacement.

4-3-2 Play inner lumen

Play between cable and articulation mechanism has the potency to provide more space for cable bending. Larger cable bends are possible under the assumption that the SATA linkages can be redesigned such that the cable can escape from its internal routing. To compare all concepts, routing play and the possibility for (partially) external cable routing are investigated. The latter aspect requires the cable to escape the internal lumen of the mechanism.

- **Concept (a):** With nested joints located at the lateral side of the instrument, no space is available for the cable to escape its internal routing.

- **Concept (b):** With nested joints located at the medial side of the instrument, sufficient space is expected for cable escape.

- **Concept (c):** Play between cable and inner lumen results in steering mechanism backlash, since the cable controls the internal DoF. Here, a paradoxical design challenge is identified, where a compromise between backlash and end-point stiffness is to be found.

- **Concept (d) - (e):** With compliant joints located at the medial side of the instrument, sufficient space is expected for cable escape.

- **Concept (f):** With elliptical flexures as designed by Dearden *et al.*[44], sufficient space is expected for cable escape. Alternatively, two counter directed flexures can be place at either side of the instrument, leaving a lumen for cable escape.

- **Concept (g) - (i):** In case of gears, the outer most teeth determine the RoM, but obstructs transmission cable escape. Likewise, cable escape is obstructed by flexure belts of a compliant rolling contact. However, for concepts (g) - (i): cable escape can be achieved with two collineair contact lines as rolling joint, such that the medial side of the joint provides a lumen for cable play. This principle is used in the compliant rolling joint developed by Herder *et al.* [2].

4-3-3 Range of Motion

According to requirement B1, $\pm 55^o$ tip articulation is needed. In the following analysis, it is discussed if this range is realistic for the concepts and their drawbacks are identified.

- **Concept (a):** When exceeding the RoM, joint dislocation occurs. In other words, the small size joint nest is a limiting factor to the range. Joint stiffness is expected to remain constant throughout the RoM.
- **Concept (b):** The relative large joint nest of this concept allows for a large RoM, because joint dislocation is not likely. Joint stiffness is expected to remain constant during motion.
- **Concept (c):** With cable deformation at the inner joint, the RoM of this concept is limited by material stress and in the long term by fatigue. Lengthening of the cable enables a larger RoM, but this same length reduces joint stiffness. Further, joint stiffness depends on the joint's characteristic radius [45].
- **Concept (d):** The lumped material compliance of a notch joint is associated with relative small rotation, which makes the joint less suitable for dynamic applications [41, 38]. However, as done in US patent No. 2013/0274741 [46], the range can be extended with multiple notch joints stacked.
- **Concept (e):** Leaf flexures offer large ranges of motion as compared to notch joints [47]. For short time utilization, the RoM of this concept is limited by yielding and for the long term it is limited by fatigue as well. Joint stiffness depends on the joint's characteristic radius [45].
- **Concept (f):** Compared to leaf flexures and notch joints, crossed flexures have a large RoM [47]. In a proof of concept, Dearden *et al.* [44] achieved 90^o tip articulation with their NiTiNol steering mechanism of ∅3mm, indicating that concept (f) is expected to have a large RoM. Limiting factors are comparable to concept (e) and stiffness depends on the characteristic joint radius [45].
- **Concept (g):** With teeth preventing slip, the range of rolling motion is limited by the edges of the toothed surface. In theory, the gear interface can reach the lateral instrument side, yielding a large RoM.
- **Concept (h):** The rolling contact of concept (h): is lost when slip occurs. With sufficient friction at the interface, a large RoM can be obtained.
- **Concept (i):** The compliant rolling contact comprises flexures with constant curvature, yielding constant stresses in the flexures throughout motion [42]. Consequently, the characteristic joint radius and thus joint stiffness remain constant.

4-3-4 Force resistance

Axial loads applied to the internally routed cable result in reaction forces in the articulation mechanism. These forces can cause motion of the mechanism's internal DoF that must be kinematically stabilized by the inner joint.

- **(a) -(b):** The rigid interface of nested joints offers high force resistance. Production tolerances can can result in backlash.
- **Concept (c):** Using the transmission cable as inner joint gives rise to a paradoxical design problem where a compromise is to be made between being stiff for force resistance and being flexible to adopt a required shape, a compromise also seen in endoscopy [48].
- **Concept (d):** Force resistance of compliant joints depends on joint geometry. In general, lumped compliant joints provide more stiffness as compared to distributed compliant joints [38].
- **Concept (e):** A study on a leaf flexure based laparoscopic steering mechanisms has shown that leaf flexures can provide either high force resistance or a large range of motion [49]. For articulation angles above 55^o, concept (e) is not expected to provide sufficient force resistance.
- **Concept (f):** The crossed flexure configuration in concept (f) constrains the internal DoF of the steering mechanism, since one of the flexures is loaded with a tension force upon tip articulation.
- **Concept (g):** Rigid gear teeth offer high force resistance. Unintended motion is caused by backlash only.
- **Concept (h):** With slip prevented by friction, concept (h) is expected to achieve low force resistance. To obtain sufficient friction force to prevent unintended motion, high normal forces at the joint interface are needed. Design complexity is likely to increase, since some form of joint tensioning solution is needed. Note that high forces increase wear rate.
- **Concept (i):** Herder *et al.* [2] developed a steerable 5mm arthroscopic instrument capable of routing an internal cable loaded by axial forces in the same order of magnitude as in the present study. Therefore, concept (i) is expected to achieve sufficient force resistance.

4-3-5 Robustness inner joint

Wear, environmental conditions or variation in production processes affect component tolerances. To estimate system robustness, it is discussed how well the concepts perform with an uncertainty in component tolerances.

- **Concept (a):** Tolerances can induce joint clearance, resulting in backlash or even joint dislocation. In case of dislocation, the joint is expected to relocate upon actuation.
- **Concept (b):** Robustness comparable to concept (a), but due to the large joint nest, dislocation is less likely.
- **Concept (c)-(f):** With compliant joints, phenomena such as backlash are absent in concept (c)-(f). Tolerances due to production result in a slight difference in joint properties (e.g., RoM and stiffness).

- **Concept (g):** Tolerances are likely to induce backlash. In the worst case, teeth skipping occurs and kinematic relations are disturbed. In contrast to concept (a), relocation of the joint upon actuation is unlikely.
- **Concept (h):** Due to tolerances, normal force at the joint interface can be reduced, causing joint slip. In the worst case, joint dislocation occurs.
- **Concept (i):** With compliant joints, production tolerances can result in a slight difference in joint properties (e.g., RoM and stiffness).

4-3-6 Hidden surfaces

The ASTM Committee F04 on Medical and Surgical Materials and Devices proposes component disassembly to expose surfaces as measure for inherent safety by design [3]. Two design features determine the surface exposure. Firstly, SATA linkages consist of hidden surfaces inside the hinges that cannot be exposed. Thus, concepts with a single SATA linkage have a lower number of hidden surfaces. Secondly, inner joint design determines if the tip can be disassembled from the instrument shaft. Therefore, it is analyzed whether inner joint design allows for mechanism (dis-)assemblage.

- **(a)-(b):** Since nested inner joints have a loose fit that allows for joint split, the steering mechanism can be disassembled to exposes surface for cleaning.
- **Concept (c):** With a dismounted transmission cable, surfaces of the steering mechanism can be exposed for cleaning.
- **Concept (d) - (f):** The monolithic design of concept (d)-(f) is problematic to instrument modularity, hence some form of modular joint interface is needed within the frame. For instance, if the inner joint is fabricated on a tubular component, it can be hold in between frame and tip by form fit.
- **Concept (g):** ASTM guidelines dissuades gears since a fluid meniscus can be supported between narrow teeth [3]. Therefore, this concept is considered unfeasible for reprocess.
- **Concept (h):** Since rolling inner joints have a loose fit that allows for joint split, the steering mechanism can be disassembled to expose surfaces for cleaning.
- **Concept (i):** The interfaces between flexure belt and roller contain a narrow gap that can support a fluid meniscus, which is hazardous to patient safety [3]. A modular mechanism requires detachable joint interfaces, which significantly increases design complexity and seems unfeasible for the compliant technology.

4-4 Concept selection

The performed analysis provides insights on assumed performance of each concept. In general, it expected that distributed compliant inner joints (concepts (c), (e) and (f)) facilitate the smallest cable curvatures, since these mechanisms are based on material bending. Moreover, as compared to conventional joints, compliant joints do not suffer from (wear induced) backlash, joint dislocation, or slip [14, 50]. The force resistance of compliant joints depends on joint geometry and material properties [41]. Critical design factors are flexure yield strength, material fatigue limit, joint modularity and the compromise between a high force resistance and a large range of motion.

Comparing concept (e) with concept (f), a clear distinction can be made in inner joint geometry. The parallel configuration of leaf flexures either offer a large range of motion or high resistance to lateral forces when used as laparoscopic articulation mechanism [49]. Here, a paradoxical design challenge arises between design for force resistance and range of motion. This challenge is not present in concept (f) due to the crossed orientation of the flexures that results in an axial force at the flexures when external loads are applied. This makes concept (f) more likely to meet the design requirements.

Regarding the drawbacks of concept (f), it is hard to design for instrument modularity. Figure 4-2 shows a conceptual design of a detachable cross-flexure interface. With shafts sliding over one another during assembly, flexures are axially loaded and buckling is unavoidable. Therefore, an inner joint based on flexures is considered unlikely to meet all design criteria. Additionally, regarding to manufacturing, it is likely that the design is complex to produce [44].

Component robustness and manufacturability seem less critical to the conventional joint designs due to the absence of thin flexures. In Table 4-1 it can be seen that concepts (a), (b) and (g) are considered feasible to meet the design requirements. No complex designs are needed to achieve a modular joint interface suitable for (dis-)assembly. Concepts (a), (b) and (g) can be discriminated by their tendency of joint dislocation. As discussed, both concepts (a) and (g) are expected to be more prone to dislocation, than concept (b).

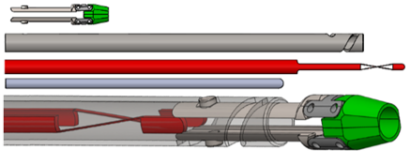

(a) Components to be assembled: (from top to bottom) SATA tip, SATA outer shaft, shaft attached inner joint and inner shaft. (bottom) detailed view of the inner joint and sliders

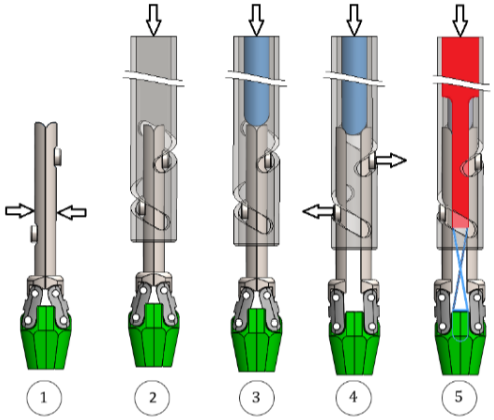

(b) Assemble procedure: (1) SATA sliders are brought together. (2) Tip is placed in SATA outer shaft (2). (3) Inner shaft is inserted. (4) Inner shaft spreads sliders. (5) Inner joint is positioned.

Figure 4-2: Conceptual design of detachable compliant inner joint.

4-5 Selected concept

Concept (b) (Figure 4-3) is selected for elaboration because of its promising mechanical performance and expected design simplicity suitable for (dis-)assembly. This concept comprises rigid components only and allows for axial split of the inner joint, making the concept suitable for (dis-)assembly. The inner joint is attached to the inner shaft and can be used to spread the SATA sliders during assembly. In other words, no extra components are needed for the intended assembly procedure (depicted in Figure 4-4). During operation, both SATA linkages prevent axial split.

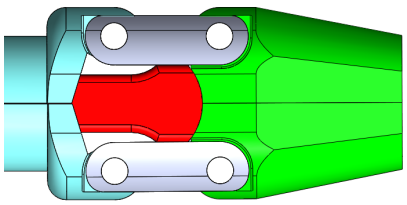

Figure 4-3: Selected concept

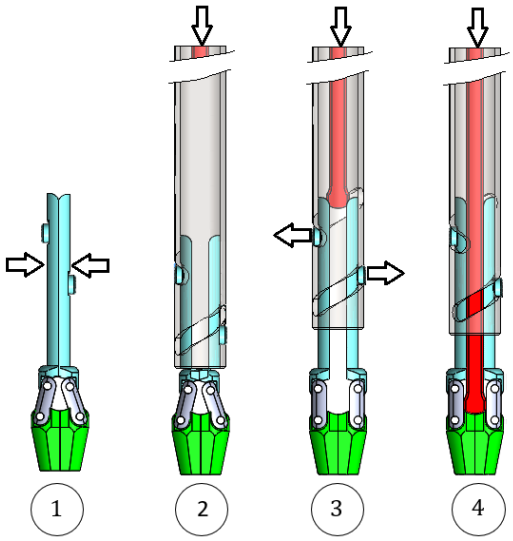

Figure 4-4: Intended assembly procedure selected concept. (1) SATA sliders are brought together. (2) Tip is inserted in SATA outer shaft. (3) Inner shaft spreads SATA sliders. (4) Inner shaft is brought in final position.

Conclusion

Concept (b) is selected for elaboration because of its promising mechanical performance and expected design simplicity suitable for (dis-)assembly.

Chapter 5

Concept elaboration

The selected concept (b), presented in previous chapters, consists of two sliders driven by the SATA outer shaft, two SATA linkages, a nested inner joint, and an instrument tip. Elaboration of the concepts is initiated by a number of design decisions regarding the topology of the nested joint. Figure 5-1 depicts the crucial design parameters that are quantified in the present chapter. These parameters are the effective tip length (L_a) (measured between tip CoR and tip hinges), length of both linkages (L_b) and the spacing between tip hinges (w).

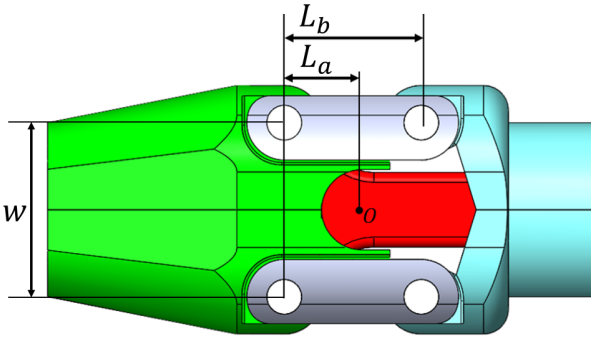

Figure 5-1: Crucial design parameters and joint center of rotation in point O.

5-1 Evolution of the nested joint

Evolution from conceptual solution to final design is schematically shown in Figure 5-2. The nested joint consists of a convex and concave joint surface that slide over one another, causing tip articulation around the CoR. The curved surfaces allow for lateral force resistance [14] and can make an angle up to 180^o, without obstructing axial joint split needed for (dis-)assembly (Figure 5-2-b). Extension of the joint nest results in a thin walled tip, therefore, material is added to the tip by reducing the size of the convex joint surface (Figure 5-2-c). Lengthening effective tip length (L_a) results in an amplification of lateral tip motion, which potentially increases cable bending radius (Figure 5-2-d).

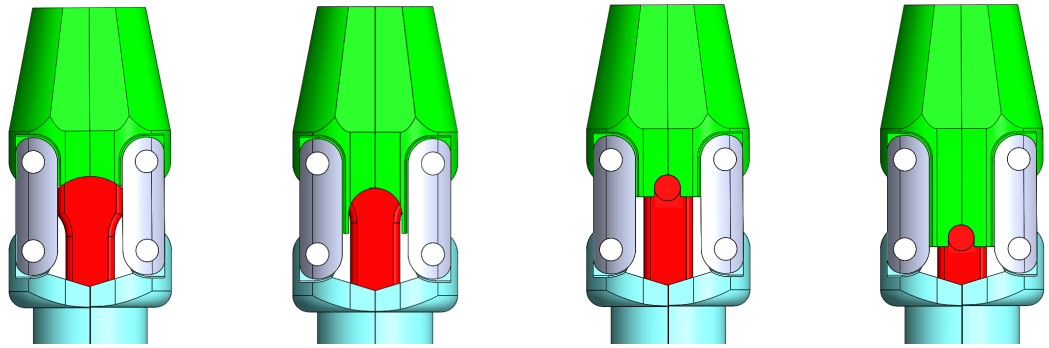

(a) Original concept.

(b) 180^o surface curvature.

(c) Material added to tip

(d) Final concept with increased effective tip length.

Figure 5-2: Evolution of nested joint design

5-2 Kinematic optimization

Articulation range is limited by mechanism jamming, as the extended tip collides with either linkage. Therefore, slider motion is optimized to avoid contact between tip and linkages. To simplify calculations, half RoM is analyzed ($0^o \leq \theta \leq \theta_{max}$). A distinction is made between inner bend linkage and outer bend linkage. It is targeted to obtain slider displacements such that the linkage in the outer bend remains parallel to the tip throughout RoM (Figure 5-3), since the parallel configuration between linkage and tip potentially leads to the largest range of motion. Let δ_{out} be the slider displacement at the outer bend directed towards the tip and let δ_{in} be the slider displacement at the inner bend directed towards instrument shaft, then Equations (5-1) to (5-3) describe the parallel motion of tip and outer bend linkage.

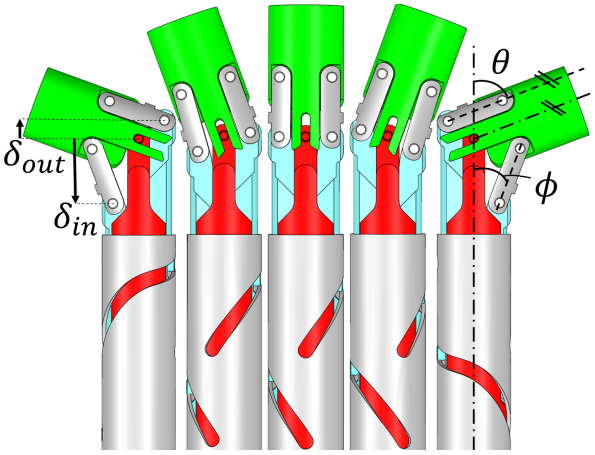

Figure 5-3: Parallel configuration between tip and outer bend linkage throughout range of motion. (left:) slider displacement indicated at maximal articulation. (right:) relevant angles indicated at maximal tip articulation.

$$\delta_{out} = L_a cos(\theta) + \frac{w}{2} sin(\theta) - L_b cos(\theta), \qquad 0^o \leq \theta \leq \theta_{max} \tag{5-1}$$

$$\delta_{in} = L_a cos(\theta) - \frac{w}{2} sin(\theta) - L_b cos(\phi), \qquad 0^o \leq \theta \leq \theta_{max} \tag{5-2}$$

Where w is the lateral spacing between hinges. Notice that the outer bend linkage rotates an angle ϕ, depending on mechanism geometry and articulation:

$$\phi = sin^{-1}\left(\frac{L_a sin(\theta) - \frac{w}{2}(1 - cos(\theta))}{L_b}\right), \qquad 0^o \leq \theta \leq \theta_{max} \tag{5-3}$$

For a parallel orientation, the effective tip length must decrease with the angle of articulation, as described by (5-4). This is made possible by allowing axial split of the joint and results in transformation of the nested joint surface to the open slotted camming surface depicted in Figure 5-4. In the remainder of the report, this feature is referred to as the joint fork.

$$L_a = \frac{L_b sin(\theta) - \frac{w}{2}(1 - cos(\theta))}{sin(\theta)}, \qquad 0^o \leq \theta \leq \theta_{max} \tag{5-4}$$

To cover the full range of motion ($[-\theta_{min}, \theta_{max}] \supseteq [-70^o, 70^o]$), slider displacement is mirrored around $\theta = 0^o$. Given the linkage length (discussed in Section 5-3), this results in the slider displacements shown in Figure 5-5.

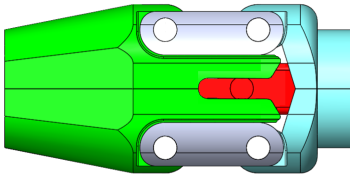

Figure 5-4: Joint fork: an open slotted camming surface.

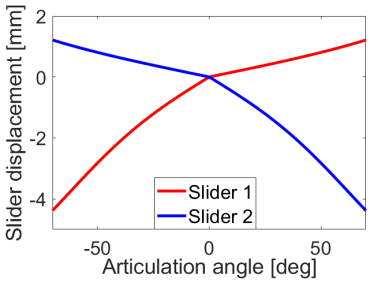

Figure 5-5: Slider displacements for a parallel configuration of linkage and tip.

5-3 Cable curvature and mechanism geometry

The circular cable curve depicted in Figure 5-6 is used to relate linkage length and cable bending radius. Relevant curve points are the Point of Curvature (PC), where cable bend begins, as well as the Point of Tangency (PT), where the cable bend terminates [51]. Tangential lines of the mentioned points intersect at the Point of Intersection (PI). Calculations are done with PI located at the instrument axis and PT at half the distance between the hinges of a maximal articulated tip (i.e., $\theta = \theta_{max} = 70^o$). The following analysis is used as starting point for cable routing design. For a gradual cable curve, contact surfaces of the internal cable route is made curcular (see Figure 5-7).

Required linkage length is calculated with Equations (5-5) to (5-7) [51]. Where x_{PI} is defined as the axial distance between PC and PI.

$$x_{PI} = \rho \cdot tan\left(\frac{\theta_{max}}{2}\right) \tag{5-5}$$

Due to symmetry around line segment PI-O, distance x_{PI} relates the lateral displacement of PT (y_{PT}) with respect to the instrument axis (Equation (5-6)).

$$y_{PT} = \frac{x_{PI}}{sin(\theta_{max})} \tag{5-6}$$

Parallel configuration between SATA tip and outer bend linkage is used in Equation (5-7).

$$L_b = \frac{y_{PT} + \frac{w}{2}(1 - cos(\theta_{max}))}{sin(\theta_{max})} \tag{5-7}$$

Substitution of Equations (5-5) - (5-7) yields a (theoretical) linkage length of 3.9mm to meet requirement B3 with a ⌀0.7mm cable that is able to support axial loads of 40N.

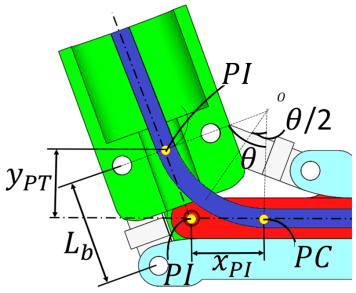

Figure 5-6: Circular cable curve (deep blue) routed through $\theta = 70^o$ articulated steering mechanism.

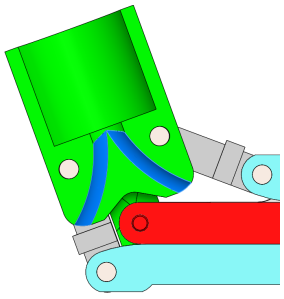

Figure 5-7: Curved surfaces (blue) to gradually guide internally routed cables.

5-4 Mechanical analysis

A static analysis of forces is presented to estimate joint reaction forces throughout the full range of motion. According to Requirement B2 (Chapter 2), grasper actuation cables can transmit forces of 40N. Thus, when grasper jaws at the tip are closed, 40N can be applied on the steering mechanism. This force is assumed to be the dominant load exerted on the mechanism and modelled as external force (T). The direction of T is assumed to be parallel to the inner bend linkage. More details on cable forces are provided in Appendix B.

5-4-1 Static equilibrium

Calculations are simplified by assuming that cable force is applied in a direction parallel to the inner bend linkage. Figure 5-8 shows the Free-body-diagram of the SATA tip in case of maximal tip articulation. Equations (5-8) to (5-10) describe the static equilibrium of forces.

$$\sum F_x : F_1 sin(\theta) + F_2 sin(\phi) - F_3 sin(0.5\pi - \theta) - T sin(\phi) = 0 \tag{5-8}$$

$$\sum F_y : F_1 cos(\theta) + F_2 cos(\phi) - F_3 cos(0.5\pi - \theta) - T cos(\phi) = 0 \tag{5-9}$$

$$\begin{aligned}\sum M_o : &- \left(L_a \cdot sin(\theta) - \frac{w}{2} cos(\theta)\right) \cdot F_1 cos(\theta) + \left(L_a cos(\theta) + \frac{w}{2} sin(\theta)\right) \cdot F_1 sin(\theta) \\ &+ (L_a \cdot sin(\theta) + \frac{w}{2} cos(\theta)) \cdot F_2 cos(\phi) + \left(\frac{w}{2} sin(\theta) - L_a cos(\theta)\right) \cdot F_2 sin(\phi) \\ &- T \cdot sin(\theta - \phi) \cdot \left(L_a - \rho \cdot tan\left(\frac{\theta - \phi}{2}\right)\right) = 0\end{aligned} \tag{5-10}$$

Figure 5-9 shows the joint forces throughout range of motion. In case of zero articulation, the mechanism is symmetric and both linkages equally support the load applied by the internal cable. However, upon articulation, asymmetry in the mechanism causes an asymmetric distribution of joint forces. Inner joint force increases with tip articulation, whereas hinge forces decrease with articulation. Maximum joint force of 44N is found at the inner joint, whereas forces at the hinges are no larger that 20N.

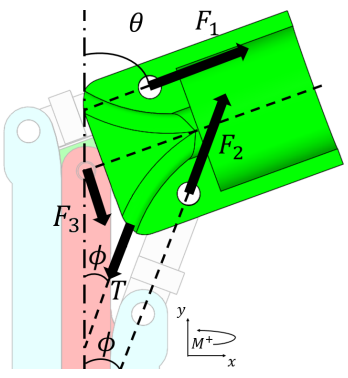

Figure 5-8: Free body diagram of tip (force T assumed to be parallel to linkage).

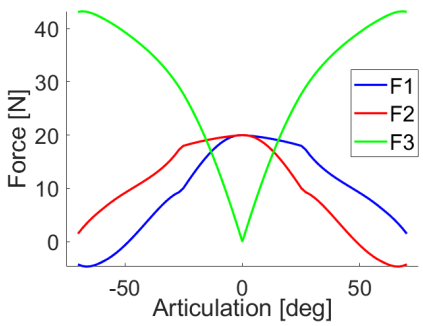

Figure 5-9: Joint forces throughout range of motion.

5-5 Outer shaft design

The outer shaft cam-follower system is redesigned to achieve desired slider motion. In principle, this system is a revolved wedge with a variable slope (Figure 5-10). Two wedges are mirrored around the shaft axis to achieve bi-directional slider motion. In this section, the revolved wedge is modelled and the transmission of mechanical load between outer shaft and tip is analyzed.

The designed slider motion is discontinuous at $\theta = 0^o$, since it is composed of two distinctive functions. To avoid abrupt changes in actuation force and to make the wedge programmable in Solidworks 2017 [52], a sixth order polynomial function is fitted (Equation (5-11), Figure 5-11). The maximum fitting error made is 0.09mm (Figure 5-12) and manifests itself in a relative angle between outer bend linkage and tip. This angle does not introduce risk of mechanism jamming.

$$\delta = -0.0740\theta^6 - 0.0360\theta^5 + 0.3742\theta^4 + 0.2643\theta^3 - 1.0933\theta^2 + 1.3426\theta - 0.0860 \quad (5\text{-}11)$$

Transmission ratio ($i = \frac{M_{shaft}}{M_{slider}}$) between the torsion applied by either slider (M_{slider}) and actuation torsion exerted to the outer shaft (M_{shaft}) is proportional to revolved wedge pitch. The pitch is determined by the number of outer shaft rotations needed to govern the full range of articulation. Figure 5-13 depicts the variable transmission ratio (i) of the cam-follower system. A maximal torsional moment of 0.03Nm is needed to hold the tip in position (see Figure 5-14 at 27^o articulation).

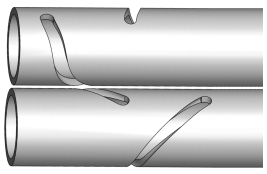

Figure 5-10: Redesigned outer shaft cam-follower system with variable slope.

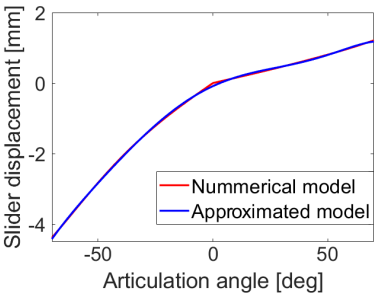

Figure 5-11: Designed slider motions. Red plot: discontinuous at zero articulation. Blue plot: continuous at zero articulation by polinomial approximation.

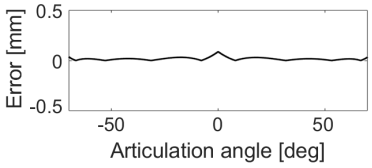

Figure 5-12: Fitting error of polynomial function.

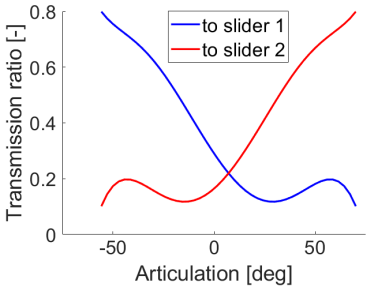

Figure 5-13: Mechanical advantage between sliders and outer shaft.

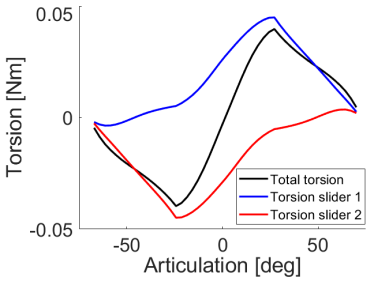

Figure 5-14: Outer shaft torsion needed to hold sliders in position upon 40N axial load at grasper actuation cable.

Summary

In this chapter, a conceptual design based on a nested joint is elaborated. Mathematical expressions are used to relate design parameters to the design requirements set in Section 2-4. A specific input motion of SATA sliders is designed to prevent mechanism jamming. The bending radius of the internally routed cable is increased by cable routing design and linkage length. Static forces are analyzed to quantify expected joint forces and used to redesign the SATA outer shaft.

Chapter 6

Final Design

Figure 6-1 depicts the final redesign of the SATA mechanism. The design forms a four-bar linkage mechanism, comprising a number of 14 components. It includes the SATA outer shaft and Sliders to actuate the tip assembly. A set of two SATA linkages is used to articulate the tip, while an open slotted cam joint is used to stabilize the tip. This cam joint is attached to the inner shaft and is located between both SATA sliders, forming a detachable connection between instrument shaft and tip. Notice that the tip, SATA linkages, hinges, SATA sliders and Slider cams form a single assembly.

The designed four-bar mechanism has two degrees of freedom (Chebychev–Grübler–Kutzbach criterion [37]) that are controlled by two actuation inputs. The SATA outer shaft provides two distinctive forces via the optimized camming-system. Kinematic stabilization of the tip is achieved by lateral directed constraint force at the tip. The design of this constraint allows for axial split and complies with the assembly method of SATA technology [20]. In this chapter, the expected performance of the redesign is analyzed.

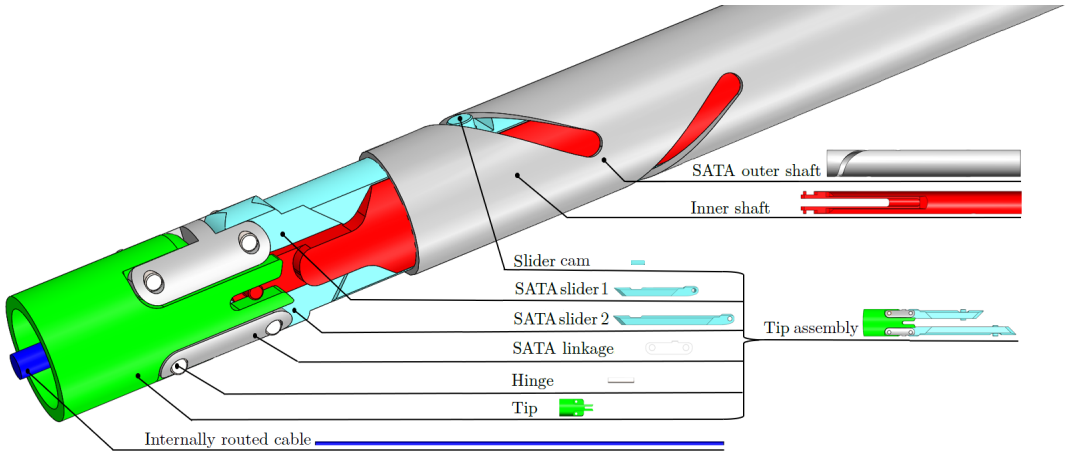

Figure 6-1: Final articulation mechanism design.

6-1 Mechanical performance analysis

Figure 6-2 and 6-3 show simplified models of the inner joint used to estimate inner joint force before material yielding. The inner joint consists of two types of interfaces: i) inner shaft attached pins and ii) tip attached slots. Crucial dimensions are the pin cross-sectional area (A), the fork length (L_f), width (b) and height (h). One interface is subjected to shear forces, and the other interface to bending loads. Equations (6-1) - (6-2) describe the material stress (σ_i) in case of shearing (V) and bending (M) loads, respectively.

$$\sigma_V = \frac{F}{A} \tag{6-1}$$

$$\sigma_M = \frac{\frac{h}{2}M}{I} \tag{6-2}$$

where A is the cross-section of the joint pin with diameter $d = 0.6$mm. To estimate forces, $M = FL_f$ and $I = \frac{1}{12}bh^3$ are substituted in Equation (6-2), with F being the joint force exerted at the fork. Calculations are based on the material properties of stainless steel grade 1.4305 (yield strength: 500MPa [53]), which is frequently used in surgical instruments [54]. Substitution of design parameters ($d = \varnothing 0.6$mm, $b = 0.85$mm $h = 0.6$mm, and $L_f = L_a - 2.65$mm) in Equation (6-1) and (6-2) yields a maximum pin force before material failure of 140N and a maximum fork force depending on the mechanism pose (see Figure 6-4). Notice that the inner joint consists of two pins and two forks, each supporting half of the mechanical load exerted at the inner joint. At 30^o articulation, the ratio between expected joint force and theoretical force before yielding is the smallest. This ratio is considered as the factor of safety and equals 2, indicating that material stresses are below (half) the yield strength.

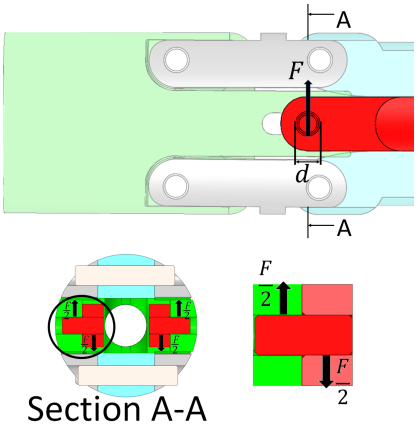

Figure 6-2: (top) Material shearing at pin. (bottom left) Cross section of inner joint. (bottom right) Simplified model.

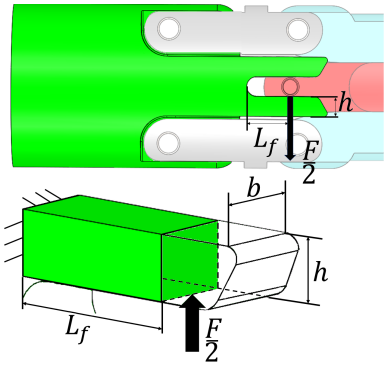

Figure 6-3: (top) Material bending at fork. (bottom) Simplified model in green.

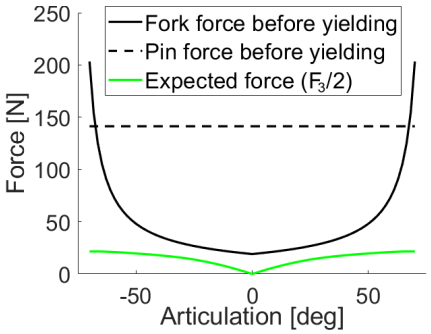

Figure 6-4: Joint forces (yield strength: 500MPa). F_3 retreived from Figure 5-9.

6-2 Kinematic performance analysis

System kinematics is subjected to stochastic variables, such as production tolerances and wear. The hazard of mechanism jamming between joint fork and inner shaft is identified. In this section, the influence of production tolerances to this hazard is analyzed based on the following tolerances:

- F7h7 fit at hinges: $|\epsilon_h| \leq 0.02$mm
- F7h7 fit at inner joint: $|\epsilon_i| \leq 0.02$mm
- Clearance sliders: $|\epsilon_s| \leq 0.025$mm
- Standard tolerance: $|\epsilon_{pt}| \leq 0.05$mm

(NEN-ISO 2768-fH [55])

As can be seen in Figure 6-5, the minimum distance (Δ) between inner shaft and tip is 0.14mm for $\theta = \pm 39^o$. In this pose, translation of the inner joint reduces clearance between tip and inner shaft, whereas rotation increases this clearance. Figure 6-6 schematically depicts critical tip motion due to production tolerances.

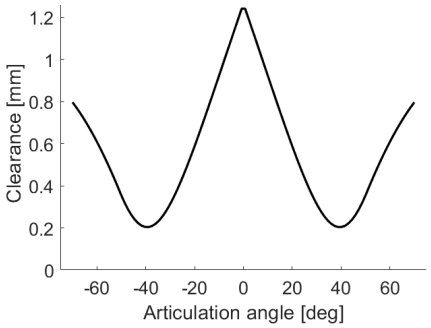

Figure 6-5: Clearance between tip and inner shaft throughout range of motion.

Clearance in all hinges cause a translation of $2\epsilon_h$ at the inner joint. Ignoring articulation, an inner joint translation of $\epsilon_s \cdot cos(\theta)$ is expected due to tolerances at either slider. Taking into account permissible deviations in nominal tip and shaft length (NEN-ISO 2768-fH), both component dimensions can have an offset ϵ_s. At the tip, deviations scale a factor $cos(\theta)$. Equation (6-3) describes the total joint translation (ϵ_{tot}) due to production tolerances.

$$\epsilon_{tot} \leq 2|\epsilon_h| + |\epsilon_s| \cdot cos(\theta) + |\epsilon_{pt}| \cdot (1 + cos(\theta)) \tag{6-3}$$

Evaluation of Equation (6-3) for $\theta = 39^o$ yields $\epsilon_{tot} = 0.15$mm. Pythagoras theorem is used to relate ϵ_{tot} to the clearance between tip and shaft. The estimated minimum clearance equals $\Delta = 0.09$mm, thus no mechanism jamming is expected.

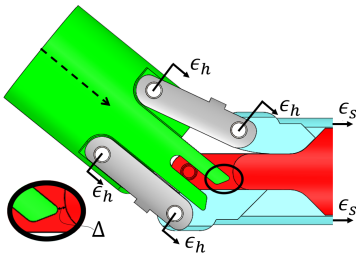

(a) Contribution of production tolerances ϵ. Dotted arrow denotes critical direction of tip displacement.

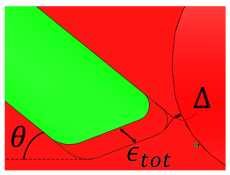

(b) Total tip displacement ϵ_{tot} by inner joint translation.

Figure 6-6: Minimal clearance (Δ) between tip and inner shaft at 39^o articulation. ϵ_{tot} being the worst case tip displacement due to production tolerances.

6-3 Risk analysis

ISO 14971 [56] defines safety as the absence of unacceptable risks. The mentioned ISO standard proposes risk control in medical instruments through inherent safety by design and suggests a risk analysis to identify hazards to control the associated risk in a systematical manner. In this section, a risk analysis is performed based on the designed steering mechanism during three different events, namely i) during production, ii) during instrument reprocess, and iii) during an electrosurgical intervention. The scope of the risk analysis is limited to risks associated with the mechanical performance of the steering mechanism. In this section, the mentioned events are analyzed and evaluated to present design measures taken for inherent safety by design.

A qualitative analysis is performed to identify hazards and to estimate both probability and severity of associated risks. Five levels of risk severity (Table 6-1) and four levels of risk probability (Table 6-2) are defined, respectively. As proposed by the University of Bath [57], the distinctive risk levels are assigned a score between 1 and 5. Multiplication of risk probability and risk severity (Table 6-3) yields the overall risk level as assigned in the three categories below. The performed risk analysis is shown in Table 6-4.

- **Highly acceptable risk:** score $1-6$
  Definition: The design is inherently safe.
- **Acceptable risk:** score $7-12$
  Definition: The design is sufficiently safe.
- **Unacceptable risk:** score $13-20$
  Definition: The design is unsafe.

Table 6-1: Risk severity level

Level	Risk severity	Rationale
1	Trivial	Neglectable effect on safety
2	Minor	Minor effect on safety
3	Moderate	Moderate effect on safety
4	Serious	Serious effect on safety
5	Unfeasible	Unsafe to use mechanism

Table 6-2: Risk probability level

Level	Risk probability	Rationale
1	Remote	Extremely rare risk occurrence
2	Occasional	Rare risk occurrence
3	Probable	Repetitie risk occurrence
4	Frequent	Frequent risk occurrence

Table 6-3: Overall risk level

	Probability Level			
Severity Level	1: Remote	2: Occasional	3: Probable	4: Frequent
1: Trivial	1	2	3	4
2: Minor	2	4	6	8
3: Moderate	3	6	9	12
4: Serious	4	8	12	16
5: Unfeasible	5	10	15	20

6-3-1 General findings

As can be seen in Table 6-4, the lowest risk level is *Acceptable*, indicating that the designed mechanism is expected to be inherently safe by design. Long term use is expected to reduce mechanism performance, which is acceptable if the condition of the mechanism is monitored [58]. For example, a hazard of long term use is corrosion, which cannot be prevented by design. In the long term, safety requires disposal of the steering mechanism, because of risks that cannot be controlled by design [59].

Table 6-4: Risk analysis

Category	Risk	Hazard	Occurrence	Severity	Overall risk level	Designed Solution
Manufacturing (CNC machining and assemble)	Low eigen frequency of features	- Workpiece resonates	Occasional	Unfeasible	Acceptable	Eigen frequency of long slender features must be lower than milling or turning frequencies
	Instrument misassembly	- Mechanism malfunction	Occasional	Unfeasible	Acceptable	Use working drawings
	Nominal lengths deviate	- Different tip kinematics - Mechanism jamming - Reduced range of motion	Frequent	Trivial	Highly acceptable	Strict ISO 2768-f tolerances used in manufacturing
	Wrong clearance fit at pins	- Transition fit - High friction in joints - Reduced mechanism precision	Remote	Unfeasible	Highly acceptable	Strict ISO 286 tolerances used in manufacturing
	Wrong interference fit at pins	- Transition fit - Dislocation of pins	Remote	Unfeasible	Highly acceptable	Strict ISO 286 tolerances used in manufacturing
	Machining burr	- Debris left in patient causing inflammation [37]	Remote	Unfeasible	Highly acceptable	Remove burr by post-processing
	Material defects	- Stress peaks - Reduced mechanism load capacity	Remote	Serious	Highly acceptable	Use certified materials and certified production methods only (ISO ISO 13485)
	High surface roughness	- High friction - Reduced mechanism precision - Microbial growth [60]	Remote	Serious	Highly acceptable	Surface finish by post-processing
	Hinges not straight	- High friction - Reduced mechanism precision - Mechanism jamming	Frequent	Trivial	Highly acceptable	Strict ISO 2768-H tolerances used in manufacturing
Instrument reprocessing	Aggressive cleaning agents used for sterilization	- Corrosion causing material deterioration [61] - Crystalline deposition causing inflammation or surgical shock [62]	Possible	Moderate	Acceptable	Limit intended life span of mechanism
	Rough handling during transport	- Damaged components - Mechanism malfunction	Possible	Moderate	Acceptable	Long slender features are avoided because of fragility
	Repeated mechanism (dis-)assembly	- Component wear - Increased clearances	Probable	Minor	Acceptable	Durable materials selected
	Misassembly of mechanism assembly	- Mechanism malfunction	Occasional	Unfeasible	Acceptable	Only one way possible to assemble components
	Improper cleaning	- Patient cross-contamination	Occasional	Unfeasible	Acceptable	- Detachable tip to expose hidden surfaces - Detachable shafts to flush lumen
	Loosing components	- Instrument malfunction	Occasional	Unfeasible	Acceptable	- Smallest components not detachable - Modular design allows for component replacement
	Time consuming sterilization	- High workload employees	Probable	Moderate	Acceptable	- Study had shown that SATA technology can be assembled within reasonable time [20]
	No inspection of instrument	- Instrument malfunction	Occasional	Moderate	Highly acceptable	- Surface exposure allows for component inspection
MI intervention	Mechanism backlash	- Reduced position accuracy	Probable	Minor	Acceptable	Component clearance controlled by tolerances
	Material fatigue	- Material failure - Mechanism malfunction	Occasional	Unfeasible	Acceptable	Safety factor introduced to avoid high stresses
	Excessive load applied	- Material yielding - Mechanism malfunction	Occasional	Unfeasible	Acceptable	Safety factor introduced to avoid high stresses
	Material wear	- Increased clearance - Foreign particles left in patient causing inflammation - Corrosion [63]	Frequent	Minor	Acceptable	Surface area of sliding interfaces are maximized to distribute wear
	Accumulation of tissue inside mechanism	- Patient cross-contamination - Mechanism jamming by blood clothing	Frequent	Minor	Highly acceptable	- Mechanism designed for cleaning - Linkage length minimized to reduce lumen exposure by tip articulation
	Mechanism hard to control	- Time consuming operation - Poor surgical outcomes	Occasional	Moderate	Acceptable	- The mechanism is controlled by the proven principle of outer shaft rotation [9, 19, 20] - The tip is placed in close proximity with its center of rotation
	High torsional moments needed to control mechanism	- Surgeon exhausted - High internal forces - High material wear rate	Occasional	Moderate	Acceptable	The outer shaft's cam-follower system can be stretched to improve force transmission
	Broken mechanism features	- Unretrieved device fragment [64] - Reduced load capacity	Remote	Moderate	Highly acceptable	- Mechanism design with a factor of safety - Due to symmetry, mechanism kinematics is maintained if one feature is broken. This allows for retraction of the instrument
	Improper material selected	- Material causes allergic reaction of patient	Frequent	Minor	Acceptable	The mechanism is predominantly made of grade 1.4305 stainless steel. Allergic reactions are very Probable [54], but the severity is neglectable since the mechanism is intended for transient use [28]
	Metal on metal contact at sliding interfaces	- High friction - Reduced mechanism precision	Frequent	Minor	Acceptable	Sliding interfaces consist of different alloys to reduce adhesion

Summary

In this chapter, a final steering mechanism design is presented and modelled. The design consists of rigid parts only and includes an open slotted joint located between two SATA linkages. The performance of the design is evaluated to predict the load capacity and to analyse the influence of production tolerances. A risk analysis is performed to assess safety of the designed steering mechanism. The performed analyses revealed that the final design concept is suitable to meet the design requirements set in Chapter 2.

Chapter 7

Validation of design requirements

Design requirements are set in Chapter 2 to secure cost and value of system performance. In this chapter, it is validated if all design requirements are met by the final design. Validation is done by evaluation of design features in Solidworks, by an experiment on a demonstrator, and by Finite Element Modelling (FEM).

7-1 Evaluation of design features

Dimensional requirements set in Chapter 2 are evaluated in Solidworks 2017 [52] and shown in Figure 7-1. The design has a maximal mechanism outer diameter of ∅5mm. This outer diameter fits within a standard trocar, thus requirement A1 is met. The internal cable route has curved surfaces with a radius of 5mm. Axial cable load causes the internally routed cable to bend around these curved surfaces. Taking into account Requirement B3, the steering mechanism is suitable to guide cables up to ∅1.1mm.

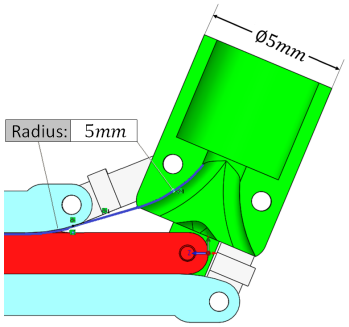

Figure 7-1: Evaluation of design parameters needed to meet design requirements.

7-2 Demonstrator experiment

Mechanism kinematics are analyzed with the 3D printed (Prusa mk3, polylactic acid) demonstrator (scale 3:1) shown in Figure 7-2. Slider displacement is analyzed with respect to the x-axis and measured from the center of the slider hinges. The analysis is performed according to a standardized test protocol provided in Appendix C. Necessary data is collected by taking photographs and processed in Solidworks 2017 to subtract the relation between slider movement and tip articulation. Matlab2018a [65] is used to fit a sixth order polynomial function in a least-squares sense for the data.

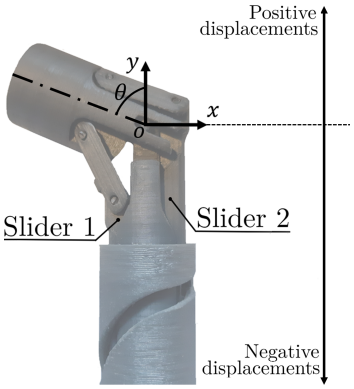

Figure 7-2: Scale 3:1 demonstrator with a coordinate system fixed at inner joint pin and an articulation angle of θ.

7-2-1 Results

Raw data and processed data are shown in Figure 7-3. Raw data shows the slider displacement of either slider at specific articulation angles ranging from -65^o to 69^o. Processed data is represented by the regression model and plotted together with the designed slider motion.

7-2-2 Interpretation and discussion

The regression model shows the same characteristics as the designed slider motion with a maximal offset of 0.5mm (Figure 7-4), reasonable considering the demonstrator is 3D printed. Intended tip articulation of $\theta = \pm 70^o$ was not achieved, likely because residual support material at the outer shaft's cam-follower system. Errors in the demonstrator originate from print resolution, residual support material and joint clearances. Errors in the measurements are induced by barrel distortion of the lens, pixel resolution, and misalignment between prototype and camera. This experiment validates that Requirements B1 and B4 are met.

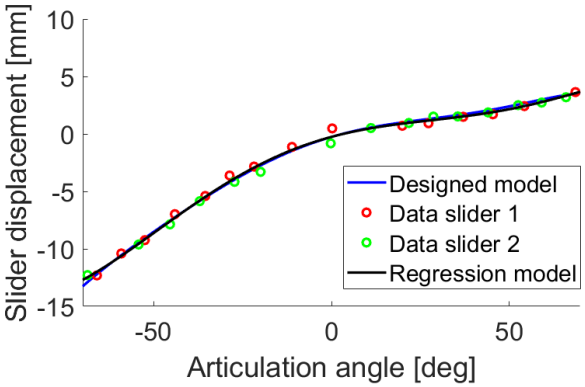

Figure 7-3: Experimental results slider motion.

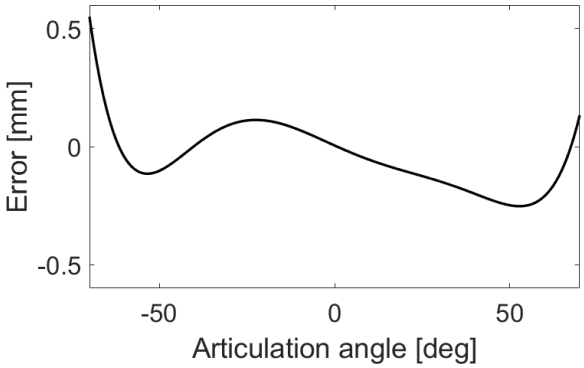

Figure 7-4: Offset between regression model and designed slider model.

7-3 Numerical evaluation

Performance of the design under 40N load at the tip is numerically approximated with a finite element model (FEM) in Solidworks 2017. This section presents the properties and simplifications of the FEM, the approximated stress distribution in the mechanism, and a discussion on obtained results. This analysis is performed to validate that Requirement B2 is met.

7-3-1 Model definitions

Figure 7-5 depicts the boundary conditions used in this analysis. The constitutive relation between stress and strain is described by Hooke's law [63]. All components are made of stainless steel alloys, therefore a Young's modulus of 200GPa is taken. A no-penetration condition is given to all component interfaces and friction forces are ignored. Fixed boundary conditions are set at the proximal side of the inner shaft and at the camming surface of either slider. External load is applied at the tip and modelled with 40N as total load directed parallel to the instrument axis. The model is meshed by triangular elements (refined at joints and edges) and the default FFEPlus solver type is used to converge to a unique solution.

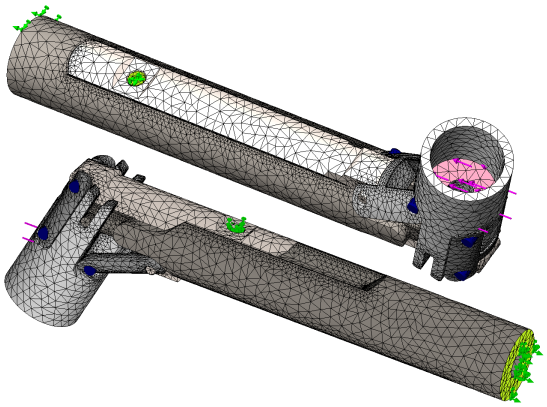

Figure 7-5: FEM boundary conditions: fixed constraints at green areas and external load at purple area in direction of purple vectors.

7-4 Modelling accuracy

Simplifications made in the presented FEM model affect numerical results. In this section, the impact of three model definitions on the numerical results is presented.

At first, with Hooke's law assumed as constitutive relation between stress and strain, only linear elastic material behavior is modelled accurately. At contact interfaces between distinctive components, non-linear material behavior is expected, leading to an inaccurate numerical approximation of contact stresses.

Secondly, the load modelled at the tip is a simplification of forces applied at the steering mechanism during a surgical procedure. The modelled load represents cable forces exerted on the steering mechanism when the grasper jaws at the tip are closed. The modelled load case in this FEM model slightly differs from the load case modelled in Chapter 5-4 and exerts a larger moment around the inner joint. It is expected that tip loads modelled in the FEM analysis result in an over estimation of material stresses stresses.

Thirdly, reaction forces of two hinges and the inner joint are in static equilibrium with the externally applied force at the tip. Considering that friction forces oppose motion, the assumption of a zero friction mechanism leads to higher joint forces.

7-4-1 Results

Figure 7-6 shows the Von Mises stress distribution in the steering mechanism for different mechanism configurations. For zero articulation, the tip load is equally supported by both linkages. Upon articulation, the load is non-uniformly distributed over the linkages and inner joint. Initially, stresses at the inner joint fork increase with an increase in articulation angle. For articulations above 40^o, fork stresses reduce with the angle of articulation.

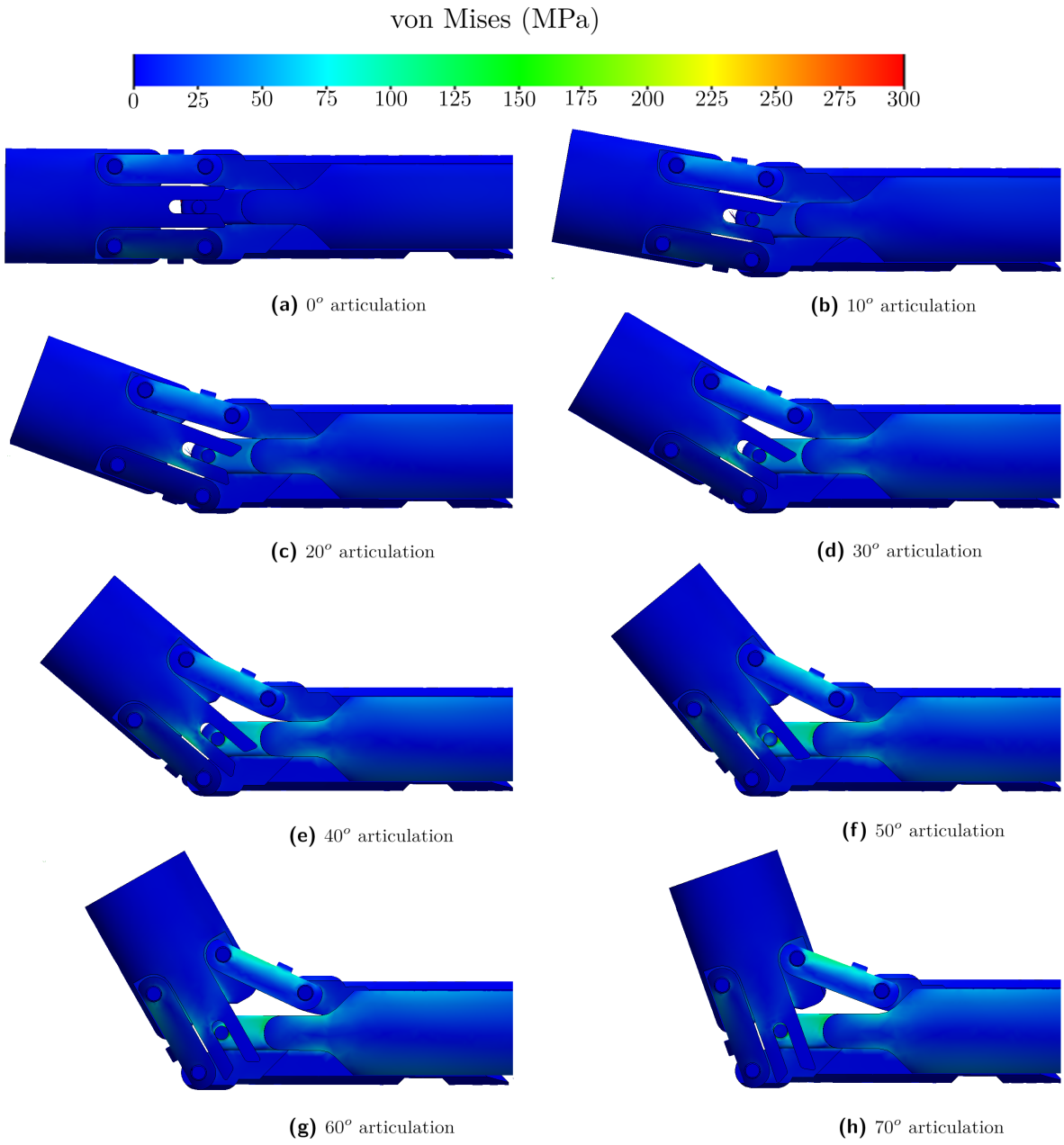

(a) 0^o articulation

(b) 10^o articulation

(c) 20^o articulation

(d) 30^o articulation

(e) 40^o articulation

(f) 50^o articulation

(g) 60^o articulation

(h) 70^o articulation

Figure 7-6: Results FEM analysis with 40N load applied at tip in direction of the instrument axis.

7-4-2 Interpretation and discussion

The inner joint pin shows a stress distribution related to shear forces, whereas the inner joint fork shows a distribution related to material bending (both shown in Figure 7-7). Above 50^o tip articulation, inner joint fork bending stresses reduce with tip articulation because of the shortening effect of the fork, as explained in Section 6-1. At macro scale, material stresses remain below 200MPa, which argues that Requirement B2 can be met. The numerical accuracy is estimated in the order of 10MPa by a sensitivity analysis through mesh variation. Table 7-1 shows the average stress at the surface of the inner bend linkage in case of 30^o.

Nevertheless, stress peaks in the order of material yield strength are calculated in the inner joint pin. These contact stresses highly depend on modelled contact interfaces and significantly fluctuate with small changes in the FEM model. As can be seen in Table 7-2, micro contact stress peaks do not converge to a unique solution (cause of this numerical inaccuracy presented in Section 7-4). Therefore, the performed FEM-analysis is considered unsuited to analyze contact stresses at a micro level. Thus, more effort is needed to validate that Requirement B2 is met.

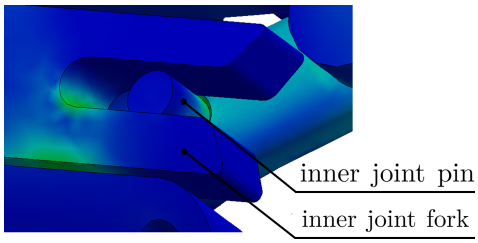

Figure 7-7: Inner joint stress: material shearing at the pin and material bending at the fork.

Table 7-1: Sensitivity analysis linkage (30^o articulation)

Mesh size	Average stress (MPa)
Coarse	22.50
Normal	23.67
Fine	24.16
Extra fine	24.73

Table 7-2: Sensitivity analysis micro contact stress (30^o articulation)

Mesh size	Peak stress (MPa)
Coarse	390.8
Normal	346.2
Fine	435.6
Extra fine	407.3

7-5 Qualitative design requirements

To ensure instrument reprocess, a number of five design requirements is set in Chapter 2. Neither of these requirements is quantifiable, therefore this section provides an overview of design measures to meet the requirements.

- *C1 - Modular design:* Redesign of SATA technology is done with an additional joint between tip and instrument shaft. This joint is designed for axial split and therefore allows for detachment (Figure 7-8). In other words, the SATA redesign is modular.
- *C2 - Prevent misassembly of instrument:* The redesigned SATA sliders have different lengths to avoid misassembly. At the inner shaft, the slider tracks have different lengths, corresponding to the distinctive sliders (Figure 7-9). A scaled demonstrator revealed that the outer shaft cannot be assembled when the sliders are positioned incorrectly.
- *C3 - Component interfaces must consist of sloping corners:* The opening of the inner joint slots are given an angle for self alignment of the inner joint pin and fork (Figure 7-10). To ease spreading of the SATA sliders inside the outer shaft, the inner shaft is given a circular surface that slides over the sloping corners of either slider (Figure 7-11).
- *C4 - No coiled cable structures are allowed in the design:* The final design comprises a number of 14 rigid components. No coiled cable structures are used for tip articulation.
- *C 5- The mechanism should be composed of autoclavable components:* All components can be produces from (medical grade) stainless steel. These components can withstand the high temperatures and humid environment of an autoclave.

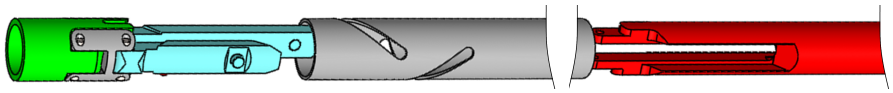

Figure 7-8: Modular design by axial inner joint split.

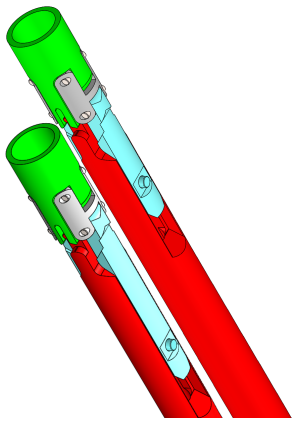

Figure 7-9: Different slider lengths.

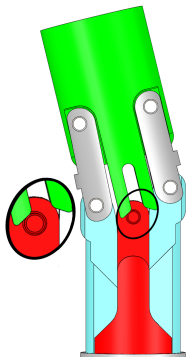

Figure 7-10: Section and detail view of sloping corners to ease assembly.

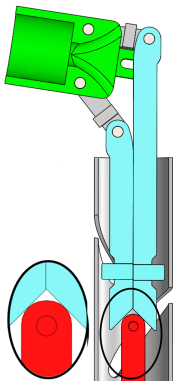

Figure 7-11: Section and detail view of sloping corners to ease assembly.

Chapter 8

Discussion and recommendation

Methods used and design decisions made in this graduation project resulted in the redesign of SATA platform technology as shown in Figure 8-1. For the redesign, a systematic bare minimum design approach is followed. In this chapter, the results of the present graduation project are discussed.

8-1 General discussion

This graduation project is initiated by the problem analysis presented in Chapter 2. The analysis is performed to obtain insights on MI steering mechanisms and instrument reprocess. One visit to the central sterilization department of the Leidsch Universitair Medisch Centrum is made to understand the procedure of instrument reprocess and ASTM guidelines are studied to attain design strategies for reusable instruments. Furthermore, state-of-the-art technologies are classified based on mechanism morphology and set in contrast with SATA technology. With this knowledge, the bottleneck in SATA technology is identified to select a design strategy. Mechanism functionalities for this graduation project are defined based on electrosurgical bipolar vessel sealing. This electrosurgical procedure is analyzed from a technical perspective as well as from a clinical perspective. To relate performance of a minimally invasive steering mechanisms to surgical outcomes, a literature study is conducted in accordance to the PRISMA method [66]. Design decisions made in this graduation project are based on this problem analysis.

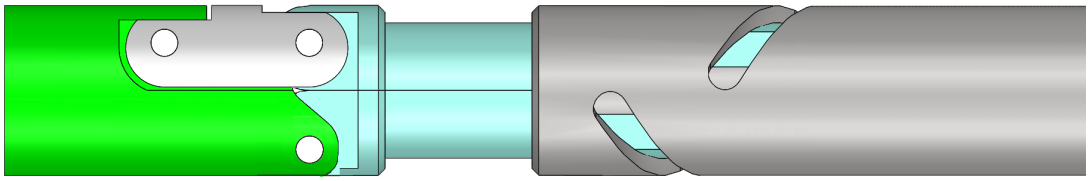

(a) Original SATA platform technology.

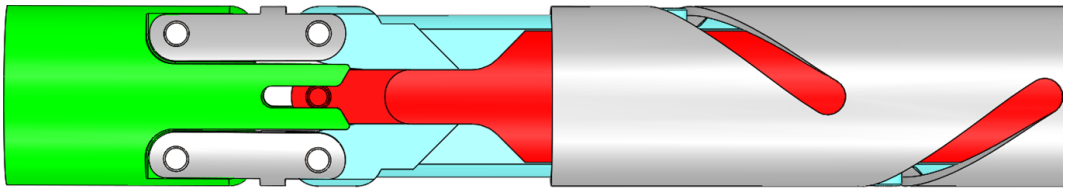

(b) Redesigned SATA platform technology.

Figure 8-1: Redesign of SATA platform technology.

Concept generation is structured by investigation of MI steering mechanism morphology and resulted in concepts inspired by backbone based steering mechanisms. Available information on concepts is generalized to form a Harris profile for substantiate concept selection. Joint detachebility is analyzed for the two most promising concepts and appeared to be a bottleneck to compliant mechanisms. A concept comprising of of rigid components is selected for elaboration, as the concept allows for axial joint split. Optimization of mechanism kinematics is done to prevent mechanism jamming in the final steering mechanism design. Mathematical expressions are used to relate design parameters to design requirements set in Chapter 2. Using a demonstrator and a FEM model, it is validated that the final design meets design requirements set in Chapter 2.

A demonstrator is built in this graduation project as proof of concept for the redesigned SATA technology, showing that the designed steering mechanism is suited for tip articulation, actuated by outer shaft rotation. The demonstrator is made out of three detachable parts and shows that the mechanism is modular, thus suited for reprocess. However, mechanical behavior of the demonstrator does not represent the behavior of the designed steering mechanism. Difference in behavior originates in scaling effects and material behavior. The first can be compensated for by scaling laws, the latter is hard to compensate for. The demonstrator is made of anisotropic polylactic acid, a stiff and brittle material, deposited layer by layer [67]. It is observed that material failure of the demonstrator occurs at the interface between layers. This failure mechanism is not present in intended mechanism material, stainless steel alloys processed by conventional machining, making the demonstrator irrelevant for experiments on mechanical load support. Therefore, it is chosen to perform a FEM analysis to obtain insights on support of mechanical loads in the steering mechanism.

The FEM analysis argued that the designed steering mechanism can support mechanical loads exerted by internally routed grasper actuation cables. However, the FEM did not converge to an unique solution of micro-scale contact stresses, because of modelling inaccuracies (Section 7-4). At the inner joint interface, convergence highly depends on set boundary conditions and mesh placement. Because of this, Requirement B2 (Chapter 2) is validated at macro scale only.

8-2 Recommendations

It is recommended to further develop the designed steering mechanism, such that it can be integrated in reusable MI instruments. The mechanism is considered as building block for MI instruments and can be placed in close proximity to an instrument tip. Furthermore, the designed mechanism allows for internal cable routing, which can be used to transmit mechanical loads between an instrument tip and the surgical handle the instruments. These loads can adopt instrument functionality in the form of graspers actuation needed for tissue manipulation, and in the form of tip rotation suitable to orientate the instrument tip with anatomic structures at the side of operation.

To further develop the steering mechanism design, it is recommended to collect more insights on contact stresses and the long-term performance of the designed mechanism. High contact stresses can limit mechanism lifespan by (sub-)surface initiated fatigue [68]. It is recommended to perform experiments on a prototype to validate if intended loads can be supported without causing early-stage fatigue. For relevant results, mechanical properties

of the prototype must represent the designed mechanism. Regarding the dimensions of the prototype, it is noticed that micro scale material stresses have a different relation with design geometry than macro scale stresses have (Appendix D). Therefore, it is recommended to produce a scale 1:1 prototype from stainless steel alloys.

Furthermore, six design aspects are deemed interesting to improve on: i) ease of instrument assembly, ii) linkage length, iii) slider length iv) the outer shaft revolved wedges, v) mechanical robustness of the inner joint, and vi) the range of motion. These possible design opportunities are presented in this section.

i) Design requirements for instrument cleaning and inspection are based on the proven concept of SATA technology [9], but, in the present study, no new insights were collected regarding instrument cleaning and inspection. Although a scaled demonstrator showed effective mechanism (dis-)assembly, it is not validated whether this can be done within a reasonable time. It is neither validated if the mechanism can be inspected or that misassembly is prevented by design. Moreover, it is recommended to produce a $1:1$ scale prototype for design validation in terms assembly and inspection.

ii) The distance between the surgical grasper and its CoR is affected by linkage length. To improve on dexterous control, this length is to be minimized [35]. A paradoxical design objective arises from the linkage length needed for cable bending, as longer linkages potentially lead to larger bending radii. In this graduation project, linkage length is based on required cable bending radius. More effort can be made to ease surgeons' control by reconsidering the linkage length.

iii) It appears that slider length significantly influences mechanism backlash. Lengthening the slider segment inside the inner shaft tempers play, but lengthening leads to long slider tracks at the inner shaft. These tracks are long slender features with a bending stiffness inversely proportional to the length to the power three ($k \propto \frac{1}{L^3}$[38]). Some stiffness of this feature is needed to avoid vibration during manufacturing by conventional machining.

iv) Regarding the outer shaft design, it was chosen to govern the full range of tip articulation with a half revolution of the outer shaft. Compared to the original SATA design, the ratio of outer shaft rotation and tip articulation is a factor 1.3 higher. Motion scaling can result in higher accuracy in positioning the instrument tip without extending the time needed to position the instrument [69]. Furthermore, considering the transmission ratio of force between outer shaft and sliders, flattening the slope of the revolved wedge results in a more favorable transmission of forces. I.e., surgeons' effort can be reduced by flattening the curve of the outer shaft. Therefore, it is recommended to consider a larger outer shaft revolution to govern the full range of tip articulation.

v) Mechanical robustness of the inner joint is limited by the space available between both SATA sliders. To increase robustness of either joint interface, a trade-off between fork thickness and inner joint pin diameter has to be made. Both design parameters scale quadratic with the maximum allowable joint force. Since the inner joint fork is found to be the most critical design feature, one can decide to increase fork height at the cost of inner joint pin diameter. Notice that the mechanical analyses performed in this graduation project were based on stainless steel grade 1.4305. For further development, it is recommended to emphasise on material selection. For instance, if the inner joint pin is made out of hardened stainless steel

grade 1.4542, maximum allowable shear force is increased by a factor 2 [70], making the joint more robust to high micro contact stresses.

vi) The range of tip articulation can be extended from $\pm 70^o$ to $\pm 90^o$, without introducing mechanism singularity. This demands a compromise in terms of internal cable bending radius, since the cable curvature becomes larger. It is recommended to analyze the waterbed effect between increased articulation and cable bending radius before extending the range of tip articulation.

8-3 Future applications

The designed steering mechanism can be considered as building block for reusable MI instruments. The design allows for internal cable routing through reusable MI instruments and can be used to add functionality to MI instruments in the form of tip articulation and tip rotation. Surgeons would benefit from these functionalities, since they retrieve additional DoFs to orientate an instrument with anatomic structures at the side of operation.

Furthermore, laser ablation instruments would benefit from the designed steering mechanism, as the mechanism can bend internally routed optic fibers with large radii. For example, the steering mechanism can be integrated in instruments used during fetosopic laser surgery. In this procedure, the steering mechanism can be used to orient optical fiber with placenta vessels (i.e., chorioangiopagous vessels) that need to be occluded by ablation. This procedure is used as treatment for twin-to-twin transfusion syndrome (TTTS) [71].

Chapter 9

Conclusion

In this graduation project, SATA platform technology is redesigned to comply with internally routed cables. These cables can be used to actuate and to rotate a surgical grasper located at an instrument tip. An additional linkage to the platform technology improves the bending radius of cables routed through MI instruments, while a novel and innovative detachable joint adds a kinematic constraint to avoid unintended tip motion. The designed 1 DoF steering mechanism is driven by rigid components only and provides tip articulation up to $\pm 70^o$. A demonstrator is built and allowed for a proof of principle for the redesign. The designed steering mechanism can be used as building block for reusable minimally invasive instruments, providing an important step to the next generation of SATA platform technology.

Bibliography

[1] Ninh T. Nguyen, Charles Goldman, C. John Rosenquist, Andres Arango, Carol J. Cole, Steven J. Lee, and Bruce M. Wolfe. Laparoscopic versus open gastric bypass: A randomized study of outcomes, quality of life, and costs. *Annals of Surgery*, 234(3):279–291, 2001.

[2] Tin Yan Nai, Just L. Herder, and Gabriëlle J. M. Tuijthof. Steerable Mechanical Joint for High Load Transmission in Minimally Invasive Instruments Steerable Mechanical Joint for High Load Transmission in Minimally Invasive Instruments. *Journal of Medical Devices*, 5(September):1–7, 2011.

[3] ASTM F3357 - 19. Standard Guide for Designing Reusable Medical Devices for Cleanability 1. *Book of Standards Volume*, 13.02:1–7, 2019.

[4] Joey Siu, Andrew G. Hill, and Andrew D. MacCormick. Systematic review of reusable versus disposable laparoscopic instruments: costs and safety. *ANZ Journal of Surgery*, 87(1-2):28–33, 1 2017.

[5] StatLine CBS. Zorguitgaven; kerncijfers. Retreived on 25-12-2020 from: https://opendata.cbs.nl/statline/#/CBS/nl/dataset/84047NED/table?ts=1608911068031, 2020.

[6] Dimitrios K. Manatakis and Nikolaos Georgopoulos. Reducing the Cost of Laparoscopy: Reusable versus Disposable Laparoscopic Instruments. *Minimally Invasive Surgery*, 2014:1–4, 2014.

[7] David Hailey, Philip D. Jacobs, Nola M. Ries, and Julie Polisena. Reuse of single use medical devices in Canada: Clinical and economic outcomes, legal and ethical issues, and current hospital practice. *International Journal of Technology Assessment in Health Care*, 24(04):430–436, 10 2008.

[8] Julien Catherine, Christine Rotinat-Libersa, and Alain Micaelli. Comparative review of endoscopic devices articulations technologies developed for minimally invasive medical procedures. *Applied Bionics and Biomechanics*, 8(2):151–171, 2011.

[9] T. Horeman, F. Schilder, M. Aguirre, G. M.M.J. Kerkhoffs, and G. J.M. Tuijthof. Design and preliminary evaluation of a stiff steerable cutter for arthroscopic procedures. *Journal of Medical Devices, Transactions of the ASME*, 9(4):1–6, 2015.

[10] J. Jänsch and H. Birkhofer. The development of the guideline VDI 2221 - The change of direction. *9th International Design Conference, DESIGN 2006*, pages 45–52, 2006.

[11] Ali Faraz and Shahram Payandeh. *Engineering Approaches to Mechanical and Robotic Design for Minimally Invasive Surgery (MIS)*. Springer US, Boston, MA, 2000.

[12] Ian A. Gravagne and Ian D. Walker. Manipulability, force, and compliance analysis for planar continuum manipulators. *IEEE Transactions on Robotics and Automation*, 18(3):263–273, 2002.

[13] J Mueglitz, G Kunad, P Dautzenberg, B Neisius, and R Trapp. Kinematic problems of manipulators for minimal invasive surgery. *Endoscopic surgery and allied technologies*, 1(3):160–164, 1993.

[14] Filip Jelínek, Ewout A. Arkenbout, Paul W. J. Henselmans, Rob Pessers, and Paul Breedveld. Classification of Joints Used in Steerable Instruments for Minimally Invasive Surgery—A Review of the State of the Art. *Journal of Medical Devices*, 9(1), 3 2015.

[15] Filip Jelínek, Giada Gerboni, Paul W J Henselmans, R O B Pessers, and Paul Breedveld. Attaining high bending stiffness by full actuation in steerable minimally invasive surgical instruments. *Minimally Invasive Therapy & Allied Technologies*, (24:2):77–85, 2015.

[16] Yong Jae Kim, Shanbao Cheng, Sangbae Kim, and Karl Iagnemma. A novel layer jamming mechanism with tunable stiffness capability for minimally invasive surgery. *IEEE Transactions on Robotics*, 29(4):1031–1042, 2013.

[17] Giada Gerboni, Paul W J Henselmans, Ewout A Arkenbout, Wouter R Van Furth, and Paul Breedveld. HelixFlex : bioinspired maneuverable instrument for skull base surgery. *Bioinspiration & Biomimetics*, 10(6):066013, 12 2015.

[18] Intuitive Surgical Inc. Da Vinci® Energy Vessel Sealer Extend. Retreived March 12 from: https://www.intuitive.com/en-us/-/media/Project/Intuitive-surgical/files/pdf/vse-brochure-1040305.pdf?la=en&hash=4E856CBE05C0DAA8B9778CFA9BFDBB70.

[19] Tim Horeman, Milton Aguirre, G. M.M.J. Kerkhoffs, J. Dankelman, and G. M.J. Tuijthof. The SATA, A simple, stiff, and rigid steering mechanism. *Journal of Medical Devices, Transactions of the ASME*, 9(3), 2015.

[20] Sem F. Hardon, Frank Schilder, Jaap Bonjer, Jenny Dankelman, and Tim Horeman. A new modular mechanism that allows full detachability and cleaning of steerable laparoscopic instruments. *Surgical Endoscopy*, 33(10):3484–3493, 2019.

[21] R.C. Hibbeler. Mechanics of Materials. In *Ninth Edition*, chapter 12, pages 573–580. Pearson Education Centre, Singapore, 2014.

[22] Ibrahim Alkatout, Thoralf Schollmeyer, Nusrat A. Hawaldar, Nidhi Sharma, and Liselotte Mettler. Principles and safety measures of electrosurgery in laparoscopy. *Journal of the Society of Laparoendoscopic Surgeons*, 16(1):130–139, 2012.

[23] Henri Clavé, Arnaud Clavé, Henri Clave, and Arnaud Clave. Safety and Efficacy of Advanced Bipolar Vessel Sealing in Vaginal Hysterectomy: 1000 Cases. *Journal of Minimally Invasive Gynecology*, 24(2):272–279, 2 2017.

[24] Andrew I. Brill. Bipolar electrosurgery: Convention and innovation. *Clinical Obstetrics and Gynecology*, 51(1):153–158, 2008.

[25] Nader N. Massarweh, Ned Cosgriff, and Douglas P. Slakey. Electrosurgery: History, principles, and current and future uses. *Journal of the American College of Surgeons*, 202(3):520–530, 2006.

[26] Michele Grieco, Daniela Apa, Domenico Spoletini, Emanuela Grattarola, and Massimo Carlini. Major vessel sealing in laparoscopic surgery for colorectal cancer: A single-center experience with 759 patients. *World Journal of Surgical Oncology*, 16(1):2–6, 2018.

[27] Marcus Overhaus, Nico Schaefer, Klaus Walgenbach, Andreas Hirner, Mara Natascha Szyrach, and René Hany Tolba. Efficiency and safety of bipolar vessel and tissue sealing in visceral surgery. *Minimally Invasive Therapy and Allied Technologies*, 21(6):396–401, 2012.

[28] Regulation (EU) 2017/745 of the European Parliament and of the Council of 5 April 2017 on medical devices, amending Directive 2001/83/EC, Regulation (EC) No 178/2002 and Regulation (EC) No 1223/2009 and repealing Council Directives 90/385/EEC and 93/42/EE. *Official Journal of the European Union*, 0.

[29] Aaron C. Voegele, Donna L. Korvick, Mario Gutierrez, Jeffrey W. Clymer, and Joseph F. Amaral. Perpendicular blood vessel seals are stronger than those made at an angle. *Journal of Laparoendoscopic and Advanced Surgical Techniques*, 23(8):669–672, 2013.

[30] Malcolm G Munro. 2. Fundamentals of Electrosurgery Part I: Principles of Radiofrequency Energy for Surgery. *The SAGES Manual on the Fundamental Use of Surgical Energy (FUSE). Springer, New York, NY*, pages 15–59, 2012.

[31] G. J. Monkman, S. Hesse, R. Steinmann, and H. Schunk. *Robot Grippers*. John Wiley & Sons, Weinheim.

[32] Penisi Osvaldo Hugo. Industrial Grippers: State-of-the-Art and Main Design Characteristics. *Handbook of Robotic Grasp*, 10(June 2014):107–131, 2013.

[33] Tom Gilb and Lindsey Brodie. What ' s fundamentally wrong ? Improving our approach towards capturing value in requirements specification. *INCOSE*, pages 926–939, 2012.

[34] R. Lether. "Bipolar Electrosurgical Graspers: A Literature Study", MSc. literature survey, Delft University of Technology. *[Internal Document]*, page 16, 2020.

[35] Aimée Sakes, Kevin Hovland, Gerwin Smit, Jo Geraedts, and Paul Breedveld. Design of a novel three- dimensional-printed two degrees-of-freedom steerable electrosurgical grasper for minimally invasive surgery. *Journal of Medical Devices, Transactions of the ASME*, 12(1), 2018.

[36] Neil Sclater and Nicholas P Chironis. Mechanisms and mechanical devices sourcebook. *Choice Reviews Online*, 49(07):49–3893, 3 2012.

[37] Grigore Gogu. Chebychev-Grübler-Kutzbach's criterion for mobility calculation of multi-loop mechanisms revisited via theory of linear transformations. *European Journal of Mechanics, A/Solids*, 24(3):427–441, 2005.

[38] Herman Soemers. Design principles for precision mechanisms. In *ISBN/EAN 9789036531030*, chapter 2, pages 41–86. Enschede, the Netherlands, 1 edition, 2017.

[39] S Kock and W Schumacher. A Parallel x-y Manipulator with Actuation Redundancy for High-speed and Active-Stiffness Applications. *IEEE International Conference on Robotics and Automation*, 3(May):2295–2300, 1998.

[40] Hiromasa Yamashita, Daeyoung Kim, Nobuhiko Hata, and Takeyoshi Dohi. Multi-slider linkage mechanism for endoscopic forceps manipulator. *Proceedings 2003 IEEE/RSJ International Conference on Intelligent Robots and Systems*, 3:2577–2582, 2003.

[41] L. L. Howell and A. Midha. A method for the design of compliant mechanisms with small-length flexural pivots. *Journal of Mechanical Design, Transactions of the ASME*, 116(1):280–290, 1994.

[42] Jesse R Cannon, Craig P Lusk, and Larry L Howell. Compliant Rolling-Contact Element Mechanisms. In *Volume 7: 29th Mechanisms and Robotics Conference, Parts A and B*, pages 3–13. ASMEDC, 1 2005.

[43] JPE PRECISION POINT. CROSS SPRING PIVOT. Retrieved on June 18 from: http://www.jpe-innovations.com/wp-content/uploads/Cross-spring-pivot.pdf.

[44] Jason Dearden, Clayton Grames, Jason Orr, Brian D. Jensen, Spencer P. Magleby, and Larry L. Howell. Cylindrical cross-axis flexural pivots. *Precision Engineering*, 51:604–613, 2018.

[45] Juan A. Gallego and Just Herder. Synthesis Methods in Compliant Mechanisms: An Overview. In *Volume 7: 33rd Mechanisms and Robotics Conference, Parts A and B*, volume 7, pages 193–214. ASMEDC, 1 2009.

[46] Marczyk, S., Pribanic, R., Farascioni, D., Taylor, E. J., and Hathaway, P., 2013, "Endoscopic Vessel Sealer and Divider Having a Flexible Articulating Shaft," U.S. Patent No. 2013/0274741.

[47] D. Farhadi Machekposhti, N. Tolou, and J. L. Herder. A review on compliant joints and rigid-body constant velocity universal joints toward the design of compliant homokinetic couplings. *Journal of Mechanical Design, Transactions of the ASME*, 137(3), 2015.

[48] Arjo Loeve, Paul Breedveld, and Jenny Dankelman. Scopes too flexible and too stiff. *IEEE Pulse*, 1(3):26–41, 2010.

[49] Jiening Liu, Benjamin Hall, Mary Frecker, and Edward W. Reutzel. Compliant articulation structure using superelastic NiTiNOL. *Smart Materials and Structures*, 22(9), 2013.

[50] Sridhar Kota and G K Ananthasuresh. Designing compliant mechanisms. *Mechanical Engineering-CIME*, 117(11):93–97, 1995.

[51] Ali R Vatankhah, Said M Easa, M Asce, and A Mahdavi. Alternative Solutions for Horizontal Circular Curves by Noniterative Methods Alternative Solutions for Horizontal Circular Curves by Noniterative Methods. *Journal of Surveying Engineering*, 139(August):111–119, 2013.

[52] SOLIDWORKS Education Edition. (2017). Version 2017 - 2018 / 2017 SP2.0. Waltham, Massachusetts: Dassault Systèmes SolidWorks Corp.

[53] Aalco Metals Ltd. Stainless Steel Grade 303 / 1.4305. Retrieved on 17 december 2020 from: https://www.farnell.com/datasheets/26031.pdf.

[54] Ulrich Heubner. *Stainless Steel – When Health Comes First*, volume 2. 2009.

[55] International Organization for Standardization. General tolerances - Part 1 Tolerances for linear and angular dimensions without individual tolerance indications. (ISO Standard No. 2768-1 1989 (E)). Retreived on 20-12-2020 from: https://www.3ppars.com/WebsiteImages/download/7807369945.PDF. 1989.

[56] International Organization for Standardization. Medical devices — Application of risk management to medical devices (ISO Standard No. 14971:2007(E)). 2007.

[57] University of Bath. Risk assessment guidance. Retreived on 1-1-2021 from: https://www.thesubath.com/pageassets/health-and-safety/risk-assessment-guidance.pdf.

[58] T. Brophy, Paul D. Srodon, C. Briggs, P. Barry, J. Steatham, and M. J. Birch. Quality of surgical instruments. *Annals of the Royal College of Surgeons of England*, 88(4):390–393, 2006.

[59] Arbeitskreis Instrumenten-Aufbereitung. *Instrument Reprocessing - Reprocessing of Instruments to Retain Value*. AKI, Mörfelden-Walldorf, 10 edition, 2012.

[60] Lisbeth R. Hilbert, Dorthe Bagge-Ravn, John Kold, and Lone Gram. Influence of surface roughness of stainless steel on microbial adhesion and corrosion resistance. *International Biodeterioration and Biodegradation*, 52(3):175–185, 2003.

[61] Fernando B. Mainier. Corrosion in surgical instruments. *IOSR Journal of Engineering*, 3(10):25–31, 2013.

[62] I. P. Lipscomb, A. K. Sihota, and C. W. Keevil. Comparative study of surgical instruments from sterile-service departments for presence of residual gram-negative endotoxin and proteinaceous deposits. *Journal of Clinical Microbiology*, 44(10):3728–3733, 2006.

[63] Michael F. Ashby and Hugh Shercliff. *Materials Engineering, Science, Processing and Design*. Elsevier Science & Technology, 2013.

[64] Robert A. Fischer. Danger: Beware of unretrieved device fragments. *Nursing*, 37(11):17, 2007.

[65] MATLAB. version 9.4.0 (R2018a). Natick, Massachusetts: The MathWorks Inc.

[66] Moher D, Liberati A, Tetzlaff J, and Altman DG. PRISMA 2009 Checklist. *PLoS Medicine*, 6:1–2, 2009.

[67] Ian Gibson, David Rosen, Brent Stucker, and Mahyar Khorasani. *Additive Manufacturing Technologies*. New York: Springer, 2 edition, 2015.

[68] Anton van Beek. *Advanced Engineering Design*. TU Delft, Delft, 6 edition, 2015.

[69] Sunil M. Prasad, Sandip M. Prasad, Hersh S. Maniar, Celeste Chu, Richard B. Schuessler, and Ralph J. Damiano. Surgical robotics: Impact of motion scaling on task performance. *Journal of the American College of Surgeons*, 199(6):863–868, 2004.

[70] NoMetalcor. Datasheet 1.4442 [datasheet]. retrieved on 26-10-2020 from: http://www.metalcor.de/en/datenblatt/34/#:~:text=1.4542%20By%20a%20precipitation%20hardening%20treatment.F%20AISI%20630%20By%20a%20precipitation%20hardening%20treatment.F%2017By%20a%20p, By%20a.

[71] Shigenori Iwagaki, Yuichiro Takahashi, Rika Chiaki, Kazuhiko Asai, Masako Matsui, Daisuke Katsura, and Shunsuke Yasumi. Experience with Flexible Endoscopes as Support for Difficult Visualization Cases in Fetoscopic Laser Surgery for Twin-Twin Transfusion Syndrome. *Fetal Diagnosis and Therapy*, 46(2):147–148, 2019.

Appendix A

Harris profile

In this appendix, an enlarged version of the Harris profile of the concept selection procedure (Chapter 4) is presented. The profile reveals concepts (e) and (f) as most promising concepts with an overall score of 11 and 12, respectively.

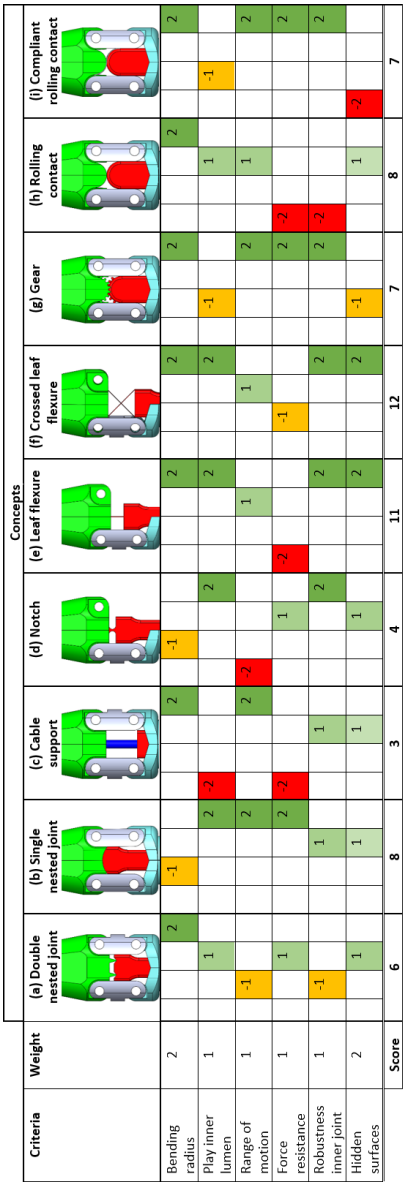

Appendix B

Details on modelled cable force

This appendix includes predicted externals loads applied at the designed steering mechanism. Assumptions are made and formulas are used to model this external load.

B-1 Expected mechanical load

In normal use, the grasper actuation cable is expected to exert the most dominant loads on the designed mechanism, any other force interaction is not analyzed. The mechanism is designed to route cables with a diameter (d) up to ∅1.1mm. This cable is guided through the mechanism with a bending radius of 5mm. Material rigidity induces a bending moment in the cable as given by Equation (Appendix B-1).

$$M = \frac{EI}{\rho} \tag{Appendix B-1}$$

with E as material Young's modulus, I as the cable's second moment of inertia (proportional to d^4), and ρ as the bending radius. Assuming that a NiTiNol cable is used ($E = 80$GPa), a cable bending moment is expected in the order of 10^{-3}Nm.This bending moment is neglected to simplify calculations, which leads to the assumption that the cable supports axial load only.

The cable is expected to exert an external force and an external moment on the designed steering mechanism. It is assumed that this load is applied at the point where cable axis is parallel to the inner bend linkage ($\phi_1 = \phi_2$), shown in Figure Appendix B-1. Based on this assumption, the effective moment arm (L_{ma}) between cable force and the Center of Rotation (CoR) of the steering mechanism is calculated.

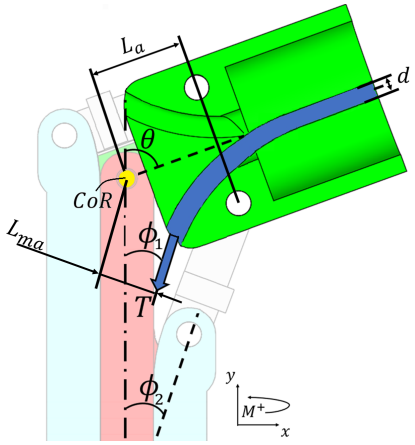

Figure Appendix B-1: Effective tip length, mechanism's center of rotation (CoR) and location of modelled cable force.

B-2 Cable model

The circular cable model depicted in Figure Appendix B-2 is used to find the effective moment arm. In the tip, the cable bends an angle β equal to $\theta - \phi$ Relevant points on the cable are the Point of Curvature (PC), the most proximal point of contact between cable and internal route in the tip. The cable bend terminates at the the Point of Tangency (PT). Tangential lines of the mentioned points intersect at the Point of Intersection (PI). The distance (L_{PI-PC}) between PI and PC is expressed by Equation (Appendix B-2) [1].

$$L_{IT} = \rho \cdot tan\left(\frac{\theta - \phi}{2}\right) \qquad \text{(Appendix B-2)}$$

The distance between mechanism CoR and point PI ($L_(C-I)$) is given by Equation (Appendix B-3).

$$L_{CI} = L_a - L_{IT} \qquad \text{(Appendix B-3)}$$

with L_a as the effective tip length measured from the CoR to the hinges at the tip (see Figure Appendix B-1). L_{C-I} is used to calculate the effective moment arm between cable force and the mechanism CoR ((Appendix B-4)).

$$L_{ma} = sin(\theta - \phi) \cdot (L_a - L_{IT}) \qquad \text{(Appendix B-4)}$$

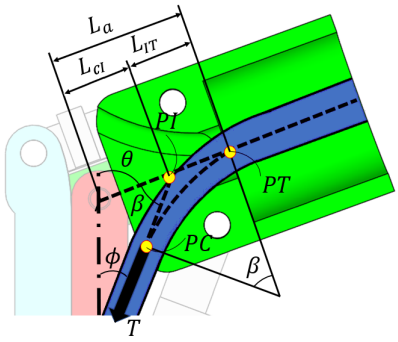

Figure Appendix B-2: Cable model used to predict loads applied at designed mechanism.

Bibliography

[1] Ali R Vatankhah, Said M Easa, M Asce, and A Mahdavi. Alternative Solutions for Horizontal Circular Curves by Noniterative Methods Alternative Solutions for Horizontal Circular Curves by Noniterative Methods. Journal of Surveying Engineering, 139(August):111–119, 2013.

Appendix C

Experimental methods

Shaft Actuated Tip Articulation (SATA) technology is an innovative type of steering mechanism used in minimally invasive surgery. Rotation of the instrument outer shaft induces linear slider motion, resulting in tip articulation (depicted in Figure Appendix C-1). In this graduation project, the cam-follower system is redesigned to allow for internal cable routing with SATA technology. This appendix describes the methodology to validate the redesigned cam-follower system.

C-1 Prototype

A scale 3:1 prototype is produced by 3D printing (Prusa mk3, polylactic acid). Clearance between components is controlled by grinding of surfaces. Hinges are made of metal pins (⌀1.2mm), fixated to the linkages by Cyanoacrylate. Motion of slider 1 and slider 2 is analyzed with respect to a body fixed frame of reference defined at the inner joint pin as shown in Figure Appendix C-2.

C-2 Experimental setup

The experimental setup is schematically shown in Figure Appendix C-3. A framework is built to mount a camera above the prototype. The camera is used to collect data and connected to a laptop to process data.

C-3 Experimental variables

The dependent and independent variables are listed below:

A Dependent variable:
- ***Displacement slider*** 1 ***(δ_1)*** depends on the angle of tip articulation.
- ***Displacement slider*** 2 ***(δ_2)*** depends on the angle of tip articulation.

B Independent variable:
- ***Angle of tip articulation*** ***(θ)*** is varied from -70^o to 70^o in steps of 10^o.

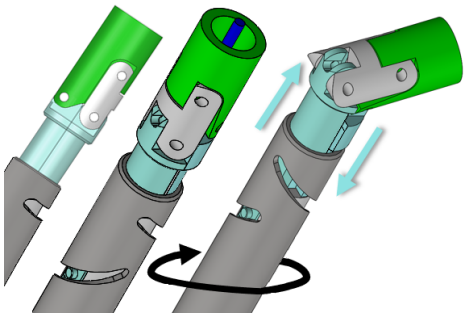

Figure Appendix C-1: Sliding motion resulting in tip articulation. Arrows indicating direction of motion.

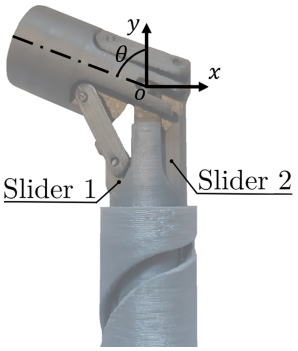

Figure Appendix C-2: Prototype with body fixed frame of reference at the inner joint pin. Angle of tip articulation is defined as θ.

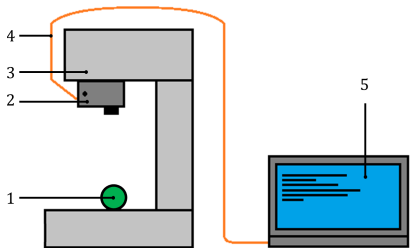

Figure Appendix C-3: Schematic representation of experimental setup. The prototype (1) is placed beneath the camera (2) mounted on a framework (3). The camera is connected by cables (4) with a laptop (5).

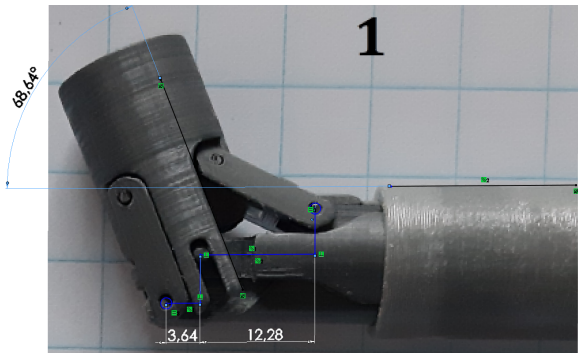

Figure Appendix C-4: Example of data processed in Solidworks.

C-4 Experimental protocol

The experiment is executed according to the standardized test protocol presented in this section. The first step is to rotate the outer shaft by hand to obtain the desired angle of tip articulation. With the tip in position, a gentle finger push is given at the distal side of the tip to compensate for clearance between components. Data is collected by taking a photograph. This sequence of actions is repeated for the angles of articulation defined in Section C-3.

C-5 Data processing

Distinctive measurements contain pixels representing the mechanism in different configurations. Data is processed in Solidworks 2017 [1] and Matlab 2018a [2] to create a scatter plot of relevant data points. This is done in the steps listed below:

1) Photographs are loaded in Solidworks and scaled such that dimensions of the prototype correspond to annotations in Solidworks drawings. These annotations are used to measure slider displacement along the y-axis and the corresponding tip articulation angles. Figure Appendix C-4 shows an example of data processed in Solidworks. This data processing step filters two relevant data points from each photograph.

2) Matlab is used to create a scatter plot of data points retrieved with Solidworks. Further, Matlab software is used to fit a sixth order polynomial function in a least-squares sense for the data.

Bibliography

[1] SOLIDWORKS Education Edition. (2017). Version 2017 - 2018 / 2017 SP2.0. Waltham, Massachusetts: Dassault Systèmes SolidWorks Corp.
[2] MATLAB. version 9.4.0 (R2018a). Natick, Massachusetts: The MathWorks Inc.

Appendix D

Scaling of material stresses

Scaling laws are important to the production of a prototype, as distribution of material stresses depends on the dimensions of the prototype. In this appendix, a dimensional analysis is performed to compare scaling laws that describe the variation of material stresses with the dimensions of the design. It is considered that design dimensions are uniformly scaled by a factor S. A comparison is made between macro-level stresses and micro-level stresses in the inner joint pin. Relevant design dimensions are the inner joint pin diameter d, pin length L_p.

D-1 Inner joint macro-level stresses

At macro-level, a joint force (F) subjects the inner joint pin to shear forces ($V = F$). The maximal material stress corresponding to this load case is described by Equation (Appendix D-1).

$$\sigma_V = \frac{V}{A} \tag{Appendix D-1}$$

The pin cross sectional area equals $A = \frac{\pi d^2}{4}$. Design dimension d is identified as scale related parameter. This reveals macro-level material stress in the joint pin to be proportional to $\sigma_V \propto S^{-2}$.

D-2 Inner joint micro level stresses

At micro-level, contact forces between pin and fork induce micro-contact stresses (σ_{mc}). Hertz's theory is used for the dimensional analyses performed in this section. For a full derivation of Hertz stresses in case of a nominal line contact, the reader is referred to [1]. Design dimensions d and L_p are identified as scale related parameters. It is found that micro-contact stresses are proportional to $\sigma_{mc} \propto S^{-1}$.

Conclusion

Variation of material stresses with design dimensions depends on the situation. At macro-level, the maximum stress in the inner joint pin is inversely proportional to the scaling factor squared. At micro level, maximal contact stress of the pin scales inversely proportional to the scaling factor of a prototype. For validation of stresses at macro and micro level, a scale 1:1 prototype is to be made.

Bibliography

[1] Anton van Beek. Advanced Engineering Design. Page 110. TU Delft, Delft, 6 edition, 2015.